ANL-AFCI-207

Argonne NATIONAL LABORATORY

Status Report on Multigroup Cross Section Generation Code Development for High-Fidelity Deterministic Neutronics Simulation System

Nuclear Engineering Division

About Argonne National Laboratory

Argonne is a U.S. Department of Energy laboratory managed by UChicago Argonne, LLC under contract DE-AC02-06CH11357. The Laboratory's main facility is outside Chicago, at 9700 South Cass Avenue, Argonne, Illinois 60439. For information about Argonne, see www.anl.gov.

Availability of This Report

This report is available, at no cost, at http://www.osti.gov/bridge. It is also available on paper to the U.S. Department of Energy and its contractors, for a processing fee, from:

U.S. Department of Energy
Office of Scientific and Technical Information
P.O. Box 62
Oak Ridge, TN 37831-0062
phone (865) 576-8401
fax (865) 576-5728
reports@adonis.osti.gov

ANL-AFCI-207

Status Report on Multigroup Cross Section Generation Code Development for High-Fidelity Deterministic Neutronics Simulation System

by
C. H. Lee and W. S. Yang
Nuclear Engineering Division, Argonne National Laboratory

September 30, 2007

work sponsored by

U. S. Department of Energy,
Office of Nuclear Energy, Science and Technology

UChicago ▶ Argonne LLC

Office of Science
U.S. DEPARTMENT OF ENERGY

A U.S. Department of Energy laboratory managed by UChicago Argonne, LLC

Table of Contents

List of Tables

List of Figures

Summary

Under the fast reactor simulation program launched in April 2007, development of an advanced multigroup cross section generation code was initiated in July 2007, in conjunction with the development of the high-fidelity deterministic neutron transport code UNIC. The general objectives are to simplify the existing multi-step schemes and to improve the resolved and unresolved resonance treatments.

Based on the review results of current methods and the fact that they have been applied successfully to fast critical experiment analyses and fast reactor designs for last three decades, the methodologies of the ETOE-2/MC^2-2/SDX code system were selected as the starting set of methodologies for multigroup cross section generation for fast reactor analysis. As the first step for coupling with the UNIC code and use in a parallel computing environment, the MC^2-2 code was updated by modernizing the memory structure and replacing old data management package subroutines and functions with FORTRAN 90 based routines. Various modifications were also made in the ETOE-2 and MC^2-2 codes to process the ENDF/B-VII.0 data properly.

Using the updated ETOE-2/MC^2-2 code system, the ENDF/B-VII.0 data was successfully processed for major heavy and intermediate nuclides employed in sodium-cooled fast reactors. Initial verification tests of the MC^2-2 libraries generated from ENDF/B-VII.0 data were performed by inter-comparison of twenty-one group infinite dilute total cross sections obtained from MC^2-2, VIM, and NJOY. For almost all nuclides considered, MC^2-2 cross sections agreed very well with those from VIM and NJOY. Preliminary validation tests of the ENDF/B-VII.0 libraries of MC^2-2 were also performed using a set of sixteen fast critical benchmark problems. The deterministic results based on MC^2-2/TWODANT calculations were in good agreement with MCNP solutions within ~0.25% $\Delta\rho$, except a few small LANL fast assemblies. Relative to the MCNP solution, the MC^2-2/TWODANT results overestimated the multiplication factor by 0.22~0.35% $\Delta\rho$ for these small systems with very hard neutron spectrum. Comparisons of measured and calculated values for the fission reaction rate ratios of Godiva and Jezebel assemblies also showed that the MC^2-2/TWODANT results agreed well with measurements within 2.7%.

From a series of methodology review and ENDF/B-VII.0 data processing, several improvement needs to enhance accuracy were also identified for the ETOE-2/MC^2-2 code system, including the multigroup slowing-down solution for whole-energy range, proper treatment for anisotropy of inelastic scattering, improved evaluation of inelastic and high-order anisotropic scattering source in RABANL calculations.

1. Introduction

As part of the Global Nuclear Energy Partnership (GNEP), a fast reactor simulation program was launched in April 2007 to develop a suite of modern simulation tools specifically for the analysis and design of sodium cooled fast reactors. The general goal of the new suite of codes is to reduce the uncertainties and biases in the various areas of reactor design activities by enhanced prediction capabilities. Under this fast reactor simulation program, a high-fidelity deterministic neutron transport code named UNIC is being developed [1]. The final goal is to produce an integrated, advanced neutronics code that allows the high fidelity description of a nuclear reactor and simplifies the multi-step design process by direct coupling with thermal-hydraulics and structural mechanics calculations.

To allow uninterrupted applicability to core design work with smooth transition from the current approach to radically advanced ones, it was decided to provide adaptive flux solution options for the whole-core neutron transport calculation, from homogenized assembly geometries to fully explicit heterogeneous geometries. The existing homogenization approach will allow rapid turn-around time for scoping design calculations and can be used on serial desktop machines. The explicit geometry approach will provide detailed modeling capabilities for design refinement and benchmarking calculations and can be utilized in parallel computational environments from small clusters to massively parallel machines. A unified geometrical framework was selected for integration with structural mechanics and thermal-hydraulics calculations. A general geometry capability using unstructured finite elements is being developed to work within the existing tools developed for structural mechanics and thermal-hydraulics, along with domain decomposition strategies for scalable parallelization.

Three solvers are being developed to solve the multigroup transport equations: PN2ND, SN2ND, and MOCFE. The PN2ND and SN2ND solvers are being developed to solve the second-order, even-parity neutron transport equation [1]. The PN2ND solver uses the spherical harmonics method in one-, two-, and three-dimensional geometries, whereas the SN2ND solver uses the discrete ordinates method in two- and three-dimensional geometries. Lagrangian and Serendipity tetrahedral, hexahedral, and prismatic triangular elements are currently available for both solvers. The method of characteristics solver MOCFE is being developed to solve the first-order neutron transport equation. The discrete ordinates method is used for the angular

discretization, and linear tetrahedral and quadratic hexahedral elements are currently available for spatial discretization.

In July 2007, work was initiated to develop accurate and efficient capabilities to generate multigroup cross sections for the various solution options of the UNIC code by simplifying the existing multi-step schemes and improving the resolved and unresolved resonance treatments. Similar to the adaptive flux solution options, it was decided to develop the system such that the user can select the level of approximation to be used in the numerical model. As an option to simplify the multi-step approaches, it is planned to investigate the direct use of fine-group cross section libraries. Elimination of intermediate steps is to be pursued by online cross section generation based on the aforementioned transport solution options and libraries of ultra-fine group smooth cross sections and resonance parameters (or point-wise cross sections). A phased approach from an offline cross section generation scheme based on the existing methods to advanced online generation capabilities was adopted to allow uninterrupted applicability to core design work. The FY07 goal was set to the development of an initial capability for investigating important physical phenomena and identifying the optimum strategies for coupling with the neutron transport code.

Based on the review results of current methods and the fact that they have been applied successfully to fast critical experiment analyses and fast reactor designs for last three decades, the methodologies of the ETOE-2/MC^2-2/SDX code system [2] were selected as the starting set of methodologies for multigroup cross section generation for fast reactor analysis. For future extension to thermal reactor applications, the methodologies of the CENTRM/PMC system [3,4] were also selected to be investigated. It is planed to use the ultra-fine group methodologies of MC^2-2 [5] for the above resolved resonance energy range and the CENTRM methodologies for the thermal energy range. For the resolved resonance energy range, three options are to be examined: ultra-fine group method of MC^2-2 with analytic resonance integrals using the narrow resonance approximation; hyper-fine group (almost point-wise) method of MC^2-2 with RABANL integral transport calculation; and point-wise resonance method of CENTRM. As a practical approach to take into account the heterogeneity effects on resonance self-shielding more accurately, improved equivalence principle and/or subgroup methods will also be investigated.

The FY07 activities at ANL were focused on revising the ETOE-2/MC^2-2 code system to be compatible with the improved nuclear data and their representations of the ENDF/B-VII.0 [6] data released in December 2006; work on the CENTRM/PMC system was performed at ORNL on a separate work package. Revision of the MC^2-2 code in FORTRAN 90 was also initiated for eventual coupling with UNIC and use in a parallel computing environment. At present, the ENDF/B-VII.0 data has been processed for major heavy and intermediate mass nuclides employed in sodium-cooled fast reactors, with various modifications of ETOE-2 and MC^2-2. Preliminary tests of the ENDF/B-VII.0 libraries of MC^2-2 have also been performed using a set of fast critical benchmark problems, including eight LANL fast critical assemblies [7], two ANL ZPR fast critical assembles [7], and six ZPPR-21 critical assemblies [8-10]. Initial conversion of the MC^2-2 code in FORTRAN 90 has also been completed. The purpose of this report is to summarize the status of progress on the ETOE-2/MC^2-2 code updates and ENDF/B-VII.0 data processing.

Section 2 presents a brief review of current multigroup cross section generation methods. A starting set of selected methodologies for multigroup cross section generation is discussed along with needed improvements in Section 3. Modifications made on the selected ETOE-2/MC^2-2 system are summarized in Section 4. The status of ENDF/B-VII.0 data processing and its initial verification and validation results are also presented. Conclusions and future work are discussed in Section 5.

2. Review of Existing Methods

The generation of multigroup cross sections from evaluated nuclear data files continues to be one of the fundamental problems in reactor physics because of the need for accurate treatment of resonance effects. The methods used for cross section processing must take into account both the resonance characteristics of intermediate nuclides (sodium, oxygen in case of oxide fuel, and structural materials like iron, chromium, nickel, etc.) and the self-shielding in fissile and fertile nuclides. The rapidly varying elastic scattering cross sections of intermediate nuclides give rise to the fine structure of typical fast reactor spectrum and require a detailed treatment. The overlapping effect resulting from neighboring resonances either from the same nuclide or from different nuclides is another challenge in fast reactor analysis. Inelastic scattering also plays an important role in fast reactors, being the major cause of neutron slowing down at high energies.

In this section, typical methods used to generate multigroup cross sections are discussed in relation to the elastic slowing down treatment and the resonance shielding calculation.

2.1 Self-shielding Factor Method

The self-shielding factor method by Bondarenko [11] is the simplest method that was widely used for fast reactor cross section generation in the 1970s. In this approach, a generalized cross section set is first prepared by calculating multigroup cross sections for a given material as a function of background cross section and temperature. Then, the cross sections for a particular composition at a given temperature are interpolated from the cross sections in the generalized set by calculating the background cross section for each material. For a selected group structure (with a typical group width of 0.1 to 0.5 in lethargy) , the self-shielding factors of each material are computed as a function of background cross section and temperature using the resonance integrals, without the overlapping terms, and the asymptotic spectrum. Instead of the overlapping terms, the background cross section infers the approximate composition dependence of the multigroup cross sections so that this scheme provides an efficient means for survey-type calculations. Typical codes employing this approach are MINX/SPHINX [12,13] and NJOY [14].

The performance of this method depends on the adequacy of the approximations used to generate the self-shielding factors. Typically, the asymptotic spectrum is determined with the narrow resonance (NR) approximation as

$$\phi(u) = \frac{\sigma_p + \sigma_b}{\sigma_t(u) + \sigma_b} = \frac{\sigma_p + \sigma_b}{\sigma_a(u) + \sigma_s(u) + \sigma_b}, \tag{2.1}$$

where σ_t = total cross section, σ_s = total scattering cross section, σ_s = potential scattering cross section, and σ_b = background cross section. In thermal reactor analysis, the NR approximation is not valid for some of the most important low-energy resonances of fertile materials. In this case it is possible to assume the validity of NR for moderator collisions, while the energy loss due to collisions with absorber atoms is neglected (infinite mass of the absorber). Then the resonance flux for this narrow resonance infinite mass approximation (NRIM) is obtained as

$$\phi(u) = \frac{\sigma_b}{\sigma_a(u) + \sigma_b}. \tag{2.2}$$

For resonances which are neither narrow nor wide, an intermediate form is deduced from Eqs. (2.1) and (2.2) as

$$\phi(u) = \frac{\lambda\sigma_p + \sigma_b}{\sigma_a(u) + \lambda\sigma_s(u) + \sigma_b}, \tag{2.3}$$

where $0 < \lambda < 1$. When $\lambda = 1$, Eq. (2.3) gives the NR expression and when $\lambda = 0$ it gives the NRIM approximation. The factor λ is called as the intermediate resonance (IR) factor or the hydrogen equivalent factor. It is one for hydrogen, and the value for other isotopes is obtained by comparing the effective cross sections of a U-238 and H mixture with those of a different mixture in which hydrogen is partly replaced by other isotope. The λ value varies with group since it depends on the resonance width.

In fast reactor analysis, the asymptotic spectrum based on the NR approximation is generally adequate for obtaining most cross sections. The elastic removal cross section, however, is sensitive to the energy variation in flux across the energy group, particularly if the group is wide relative to the mean lethargy increment per collision - a situation frequently encountered in fast reactor analysis. With the assumption of constant collision density and elastic scattering

cross section, the effective elastic scattering cross section of an isotope i in group g is determined as

$$\sigma_{eg}^{i} = \frac{\overline{\sigma}_{eg}^{i} \xi_i}{\Delta u_g}, \tag{2.4}$$

where Δu_g is the group width, ξ_i is the mean lethargy increment per collision, and $\overline{\sigma}_{eg}^{i}$ is the effective elastic scattering cross section in group g which is calculated from the infinitely dilute scattering cross section times the self-shielding factor [15]. This definition cannot take into account the dependence of the effective cross section on the location of resonance within the group. Moreover, the constant collision density assumption is not accurate in the vicinity of strong resonance because the collision density largely deviates from the constancy assumed.

To account for the deviation from the asymptotic spectrum, several algorithms have been proposed, including the posterior correction method and the improved slowing down calculation. In the posterior correction method, a corrected removal cross section of group g is calculated using the flux at $u_g' = u_g - 0.66\xi_i$ determined by assuming the slowing down density varies linearly in lethargy between groups and that it has its group average value at the mid-lethargy point of each group. Since the slowing down density is proportional to the product of the removal cross section and the flux, it is an iterative process. Convergence is obtained when the fractional change of the flux ratio ϕ_g / ϕ_{g+1} is less than a convergence criterion. The improved slowing down calculation methods are based from one side on a better representation of flux in the integral of removal cross section or on a more consistent definition of infinite dilute removal cross section. A further improvement was obtained by using the flux obtained in the hypothesis of a slowly varying collision density and a Breit-Wigner representation of the scattering resonance inside the broad group. In this way, the position of resonance in the group is explicitly taken into account. The possibility of eliminating the major drawback of the self-shielding factor method, that is, the difficulty of accounting for the interference effects of the resonances of several intermediate elements has also been investigated. It has been reported that the interference effects can be partly accounted for using a fitting procedure to define the self-shielding of the background nuclides [16].

2.2 Ultra-fine Group Method

The ultra-fine group approach was pioneered by Hummel [17] in order to account for the fine spectrum effects attributed to resonances of nuclides with intermediate atomic weights not accounted for in the earlier resonance theory. It was intended specifically for the treatment of resonance structures of the structural and metal coolant materials present in a fast reactor composition. The dominant resonances of these materials are characterized by relatively wide neutron widths insensitive to Doppler-broadening.

In this method, a detailed flux calculation is performed by dividing the entire energy span of interest into about 2000 ultra-fine groups with equally spaced lethargy width $\Delta u \cong 1/120$, approximately equivalent to half of the maximum lethargy increment per collision of U-238. Since the flux is composition dependent, the fine structure effects on the broad group cross sections are taken into account, including the effects of mutual interactions of the resonances of several intermediate nuclides. To compute the ultra-fine group flux, ultra-fine group cross sections should be prepared. The ultra-fine group cross sections can be pre-determined in various ways, including probability table and direct integration methods.

An efficient direct integration method is based on the resonance integrals within each group and the asymptotic flux attenuated due to absorption in higher-energy resonances. With the narrow resonance approximation, the resonance integral is represented in terms of the generalized J-integral, referred as J^*-integral, including the interference and overlap effects for either single or multilevel representations of resonances [18]. The J^* treatment is quite general and can be used for resolved resonance integral calculation (in the narrow resonance approximation) and for unresolved resonance calculation. Once the ultra-fine group cross section set for a given composition is generated, the ultra-fine group spectrum can be computed via the usual fundamental mode spectrum calculations utilizing the consistent or inconsistent P_N or B_N approximation. This algorithm was coded in the MC^2-2 code [5].

The continuous slowing-down approach is an alternative in which the ultra-fine group weighting spectrum is determined by solving the slowing down density equation. It is based on the rationale that the effects attributed to the relatively smooth-varying cross sections and those attributed to the sharp resonances can be treated separately, a method particularly amenable in

conjunction with the resonance integral concept. If the slowing-down density can be determined in the absence of sharp resonances, the corresponding local slowing-down density with sharp resonances and thus the local flux can also be specified via the attenuation of the former using the resonance escape probability.

One best known approximation for solving the slowing down density equation for the case of relatively slow-varying cross sections was pioneered by Goertzel and Greuling [19] using the synthetic kernel approach. Their rationale can also be viewed as a natural consequence of applying a low-order Taylor expansion to the scattering component of the collision density. By retaining the first two terms in the expansion, the resulting first order differential equation of the slowing down density can be represented in terms of moderating parameters and local cross sections. In absence of sharp resonances, such an equation can be solved readily.

Because of its importance in fast reactor applications, a great deal of improvements of the original version by Goertzel and Greuling has since been added, most notably by Stacey [20]. The improved version of Stacey was based on a low-order Taylor expansion of the total collision density, which conceptually exhibits smoother behavior than the scattering component. By so doing, the same type of first order differential equation was derived except that all moderating parameters must be redefined. For fast reactor applications, higher order Legendre moments were also included in computing the moderating parameters. In particular, this improved method has been incorporated into the MC^2-2 code as an option for computing the ultra-fine group fundamental mode spectrum in the resolved energy range.

Most of the current multigroup cross section generation codes for fast reactor analysis are based on the ultra-fine group slowing down calculation, with some variants. Noticeable examples are the MC^2-2 and ECCO codes. The MC^2-2 code performs the fundamental mode spectrum calculation in 2082 groups. Resolved and unresolved resonances are treated explicitly by the generalized J^* integral formulation based on the narrow resonance approximation including overlapping and Doppler broadening effects. Equivalence theory is used to treat the heterogeneity effect in unit cell level. For the resolved resonance range, alternative hyper-fine group integral transport calculation is an option. The ECCO code performs the slowing down calculation in 1968 groups and uses the subgroup method to determine shielded ultra-fine group cross sections. The subgroup method employed in ECCO takes into account the resonance

structure of heavy nuclides by means of probability tables. A two-dimensional lattice analysis capability based on the collision probability method is also implemented.

2.3 Equivalence Principle Method

The heterogeneity effects are typically treated via the equivalence principle method. Under the NR, NRIM, or IR approximation and the rational approximation for the collision probabilities, the heterogeneous two-region cell can be made equivalent to a homogeneous mixture. In this case, the flux in a closely packed lattice can be represented in the same functional form as that for the homogeneous media with the potential scattering cross section augmented by the so-called escape cross section. This equivalence relation originates in the fact that the absorber region is limited geometrically to the fuel region and energetically to the resonance region. A neutron can escape resonance absorption leaving this region either geometrically or energetically (scattering collision in the narrow resonance approximation). The equivalence relation consists in simulating the geometrical escape by the addition of a fictitious scattering cross section (energetic escape).

Using the Wigner's rational approximation for the escape probability with the NR approximation, the escape cross section can be represented as

$$\Sigma_e^* = \frac{1}{\bar{l}}\left\{\frac{a(1-C)}{1+(a-1)C}\right\}, \tag{2.5}$$

where $\bar{l}$ is the mean chord length, a is the Bell factor, and C is the Dancoff factor. Typically, a is set to 1.33 and 1.08 for cylindrical and slab geometries, respectively, and the Dancoff factor is approximated by a rational function of optical thickness proposed by Bell,

$$\gamma_B = 1 - C = \frac{\bar{l}_m \Sigma_t^m}{1+\bar{l}_m \Sigma_t^m}, \tag{2.6}$$

where $\bar{l}_m$ is the average chord length for the moderator (or coolant) region and Σ_t^m is the moderator cross section, taken to be constant. A significantly enhanced approximation proposed by Hummel [21],

$$\gamma = 1 - C = \gamma_B + \gamma_B^4(1-\gamma_B), \tag{2.7}$$

has been implemented in the MC^2-2 code.

The direct equivalence between the treatment of the resonance integral in heterogeneous media and that in homogeneous media can be established to various degrees of sophistication when applied in conjunction with traditional approximations to the slowing-down equation. As in the case of isolated fuel lumps, one only needs to redefine the 'equivalent' cross section Σ_e according to Eq. (2.5). For the NR approximation, it is readily amenable to the J^*-integral approach from which the multigroup cross sections can be obtained. The viability of this type of approach has been demonstrated by the MC^2-2 code. The same logic applies if one chooses to use the NRIM or IR approximation. The equivalence relation also makes possible the use of the self-shielding factor method widely employed for routine reactor calculations. For this case, the pre-computed self-shielding factors at a given temperature as a function of background cross sections are generated for various pre-selected groups and stored prior to their deployment at run time.

Many thermal reactor lattice codes (WIMS-E, EPRI-CPM, CASMO, PHENIX, DRAGOM, and WIMS-AECL) use the similar self-shielding models, with various improvements. Typically, the fuel-to-fuel collision probability is approximated by a rational function to represent its variation with respect to the microscopic total cross section of fuel. A higher order expansion is also used with several rational fractional terms in both the numerator and denominator. Recent improvements have permitted the representation of distributed effects together with an increase in accuracy. Distributed self-shielding effects are related to the spatial representation of space-dependent capture and fission rates in a specific resonant isotope such as U-238. Use of this class of self-shielding models is currently phased out, however, mainly because of the difficulty of representing modern assemblies present in advanced reactors. Accurate modeling of distributed self-shielding or mutual resonant effects are now required, and it is becoming difficult to generalize models based on rational approximation of the fuel-to-fuel collision probability [22].

2.4 Subgroup Method

The subgroup method originates from the probability table method developed by Levitt to treat the unresolved resonances [23]. In this method, the probability density function and conditional means of partial cross sections are numerically derived and tabulated as a function of total cross section. The same principle was extended for the treatment of the resolved resonances in conjunction with the subgroup (or multiband) methods developed independently by Nikolaev [24], Cullen [25], and Ribon [26].

Using the probability density function $p(\sigma)$ for the microscopic total cross section of a resonant isotope, a Riemann integral over any resonant quantity in lethargy can be replaced by an equivalent Lebesgue integral in total cross section. Thus the average of any function $f(\sigma)$ can be expressed as

$$< f >= \frac{1}{\Delta u_g} \int_{u_{g-1}}^{u_g} f[\sigma(u)]du = \frac{1}{\Delta u} \int_{\sigma_{\min}}^{\sigma_{\max}} f(\sigma)p(\sigma)d\sigma, \tag{2.8}$$

where $\Delta u_g = u_g - u_{g-1}$. By representing the probability density by a series of Dirac delta functions at discrete values σ_n, Eq. (2.7) can be approximated as

$$< f >= \frac{1}{\Delta u} \int_{\sigma_{\min}}^{\sigma_{\max}} f(\sigma)p(\sigma)d\sigma \cong \sum_n \omega_n f_n , \tag{2.9}$$

where $f_n = f(\sigma_n)$ and ω_n is the weight corresponding to σ_n. The quadrature set $\{\omega_n, \sigma_n\}$ corresponding to group g is called a probability table for the variable σ. Note that $\sum_n \omega_n = 1$ by definition. The average of a product of the type $\sigma_x f(\sigma)$ can be evaluated using the conditional probability $p(\sigma_x \mid \sigma)$ as

$$< \sigma_x f >= \frac{1}{\Delta u} \int_{\sigma_{\min}}^{\sigma_{\max}} \bar{\sigma}_x f(\sigma)p(\sigma)d\sigma \cong \sum_n \omega_n \bar{\sigma}_{xn} f_n , \tag{2.10}$$

where

$$\bar{\sigma}_x(\sigma) = \int_{\sigma_{x,\min}}^{\sigma_{x,\max}} \sigma_x p(\sigma_x \mid \sigma) d\sigma_x \,. \tag{2.11}$$

In the subgroup method, all Riemann integrals over resonant quantities in energy are replaced with Lebesgue integrals in total cross section and the Lebesgue integrals are discretized with probability tables, as described above. The resulting equation called a subgroup (or multiband) equation has the same form of the ordinary transport equation, and thus it can be solved by conventional solution schemes such as the collision probability, discrete ordinates, and characteristic methods.

In an infinite homogeneous mixture containing a unique resonance isotope with concentration N, the subgroup flux ϕ_n for an isolated, narrow resonance is given by the narrow resonance approximation as

$$\phi_n = \frac{N\sigma_p + \Sigma_{sb}}{N\sigma_n + \Sigma_{tb}}, \tag{2.12}$$

where Σ_{tb} and Σ_{sb} are the macroscopic total and scattering cross sections of the non-resonant isotopes in the mixture, and σ_p is the potential cross section of the resonance isotopes. Using these subgroup flux components, the average flux in the mixture $<\phi>$ and the type x reaction rate of the resonant $<\sigma_x\phi>$ can be computed from Eqs. (2.8) and (2.9). Thus the effective cross section of the resonant for reaction x can be represented as

$$\tilde{\sigma}_x = \frac{<\sigma_x\phi>}{<\phi>} = \frac{\sum_n \omega_n \bar{\sigma}_{xn}\phi_n}{\sum_n \omega_n \phi_n}. \tag{2.13}$$

The subgroup flux components in a heterogeneous geometry can be determined in the subgroup equation. For example, suppose that the above resonance isotope is introduced in a heterogeneity geometry composed of I regions. Then in a collision probability formulation, the level n flux in a region i can be determined as

$$\phi_{i,n} = \sum_j p_{ij,n}(N_j\sigma_{p,j} + \Sigma_{bs,j}), \tag{2.14}$$

where i and j are region indices and $p_{ij,n}$ is the reduced collision probability for neutrons born in region j and suffering collision in i. Using these subgroup flux components, the effective cross section of the resonant for reaction x in each region can be readily determined.

There are several methods proposed for computing the probability tables. These methods can be grouped roughly into two categories: mathematical and physical probability tables. The so-called mathematical probability tables are computed in such a way to preserve selected moments of the resonance cross sections. The so-called physical probability tables are typically computed by the least squares fitting of dilution-dependent self-shielded cross sections. [22]

The subgroup flux components are computed under the assumption that the resonances in the scattering sources are not correlated with the resonances in the main collision term of the transport equation. This approximation is not valid in the resolved energy domain. The subgroup approach is therefore favored for fast breeder lattice calculations where the importance of the resolved energy domain is low. For the modeling of thermal lattices, various correction methods have been proposed in the context of the existing or proposed self-shielding methodologies. Another drawback of the subgroup approach is the difficulty to account for the mutual shielding effect of overlapping resonances between different isotopes. Several correction methods have been proposed, including an iterative procedure where in the calculation of the self-shielded cross sections of an isotope, all the other isotope cross sections are kept constant using the previous iteration values. [14,20]

2.5 Rigorous Numerical Treatment of Resonance Absorption

All the resonance integral methods have various degrees of inherent limitations. In general, there are two limitations in common. First, the rigor in the treatment of the slowing down equation is lacking especially when resonances of many nuclides are present. Secondly, the range of integration is generally taken from minus infinity to infinity without proper consideration of the finite group structures in conjunction with the multigroup applications downstream. This gives rise to the so-called “boundary effects.” To overcome these limitations and to account for heterogeneity effects of reactor lattices accurately, more rigorous methods were developed to treat resolved resonances.

One approach is the so-called "hyper-fine group" method implemented in the RABANL integral transport option of the MC^2-2 code. In this method, a given scattering interval is divided into many equally spaced hyper-fine groups with a width much smaller than the extent of the resonances under consideration. The hyper-fine group width is set to be less than one quarter of the Doppler width. This approach is, in principle, rigorous so long as the slowing down equation is valid. This hyper-fine group calculation capability is available for cylindrical unit cells and slab geometry unit cells with many plates. The cylindrical unit cell formulation is based on the transmission probabilities and interface currents at the interface of each annular region and the escape probabilities from a region to its immediate neighbors. The transmission and escape probabilities are computed under the cosine current approximation. For the slab geometry unit cell calculation, a more rigorous method without resorting to the cosine current approximation is used.

Another noticeable approach is the pointwise cross section method implemented in the CENTRM code developed for thermal reactor analysis. In this method, one-dimensional transport calculations are performed for the resolved resonance energy region using pointwise cross sections (in energy). Pointwise cross section data are prepared at different temperatures such that the cross sections between tabulated values can be interpolated accurately as a linear function of energy and the square root of absolute temperature. The overall slowing down calculation is performed in a combination of pointwise and multigroup calculations. The whole energy range is divided into three intervals: upper multigroup range, pointwise range, and lower multigroup range. By dividing the whole energy range into three intervals, pointwise transport calculations are carried out for the middle energy interval where the important absorber nuclides have resolved resonances, and multigroup calculations are performed for the upper and lower energy intervals where cross sections show smooth variations. By selecting an appropriate value for the boundary between lower and middle energy intervals, the thermal scattering of important bounded moderators such as water and graphite can be included in the pointwise calculation. Within the pointwise energy range, the slowing-down source due to elastic and discrete-level inelastic scattering reactions is computed using the pointwise flux and the scattering kernel based on the neutron kinematic relations for s-wave scattering. Continuum inelastic scattering is approximated by an analytic evaporation spectrum and assumed isotropic in the laboratory system. The multigroup cross sections in the unresolved resonance range are prepared using the

Bondarenko method with a simple analytic expression of spectrum derived from the narrow resonance approximation. Since the transport calculation is limited to one-dimensional pin cell, Dancoff factor is used to correct the escape probability in a complicated heterogeneous geometry.

For more detailed two-dimensional transport calculation, the CENTRM methodologies have been combined with the two-dimensional transport solver of NEWT [27] and implemented into the GEMINEWTRM code [28]. Typically, more than 30,000 energy points are used in the resonance energy range and more than 10,000 spatial meshes are specified for the typical thermal reactor assembly in the two-dimensional geometry. It was reported that in a typical two-dimensional thermal reactor assembly calculation, the memory requirements were greater than 3 Gbyte and the computation time with a single CPU at CPILE Linux cluster at ORNL was more than 10 hours for a single depletion step.

3. Starting Set of Methodologies

The status review of multigroup cross section generation methods summarized in Section 2 indicates that the ultra-fine group slowing-down and hyper-fine group integral transport methods implemented in the MC^2-2 code are still state-of-the-art technologies for fast reactor analysis. However, its one-dimensional pin cell calculation is not adequate for accounting for multi-dimensional heterogeneity effects accurately. The subgroup method appears to be a more promising method for treating multi-dimensional heterogeneity effects. The pointwise transport method of the CENTRM code is a rigorous resonance self-shielding method, but it is practically limited to pin cell calculations at the moment.

Based on these observations and the successful application to fast critical experiment analyses and fast reactor designs for last three decades, the methodologies of the ETOE-2/MC^2-2/SDX code system were selected as the starting set of methodologies for multigroup cross section generation for fast reactor analysis. For future extension to thermal reactor applications, the methodologies of the CENTRM/PMC system were selected to be investigated. It is planed to use initially the ultra-fine group methodologies of MC^2-2 for the above resolved resonance energy range and the CENTRM methodologies for the thermal energy range. For the resolved resonance energy range, three options are considered: ultra-fine group method of MC^2-2 with analytic resonance integrals; hyper-fine group integral transport method of MC^2-2; and point-wise transport method of CENTRM. As a practical approach to take into account the multi-dimensional heterogeneity effects accurately, improved equivalence principle and/or subgroup methods are to be investigated.

In this section, the methodologies implemented in the ETOE-2/MC^2-2 system are described, and necessary improvements are discussed, focused on enhancing the accuracy and efficiency.

3.1 ETOE-2/MC^2-2 Methodologies

The ETOE-2 code processes the fundamental nuclear data from ENDF/B data file to prepare isotopic binary library files for use in the MC^2-2 code. The ETOE-2 code performs the following five basic functions: (1) reformat the data, (2) preprocess resonance cross sections by

converting Reich-Moore parameters to multi-pole parameters and by screening extremely wide and weak resolved resonances, (3) generate ultra-fine-group smooth cross sections, (4) calculate isotope-independent function tables, and (5) convert all ENDF/B formats to the laws which are allowed by MC^2-2 and RABANL. The binary data files provided by the ETOE-2 code contains resolved resonance parameters, unresolved resonance parameters, ultra-fine group smooth cross sections, inelastic and (n,2n) scattering data, fission spectrum parameters, elastic scattering distributions, isotope-independent function tables, and an administrative file. The process generating isotopic MC^2-2 libraries in ETOE-2 is depicted in Figure 3.1.

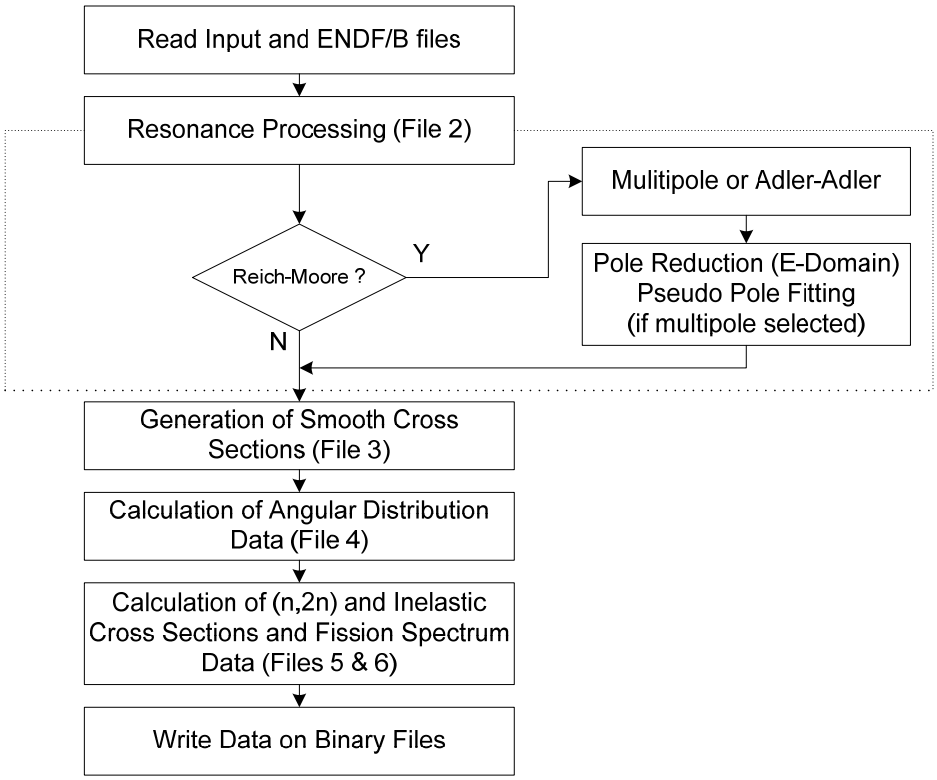

Figure 3.1 Generation of Isotopic MC^2-2 Library in ETOE-2.

One of the important options available in ETOE-2 is to screen out some resolved resonances into composition- and temperature-independent ultra-fine group (typically a constant lethargy of 1/120) smooth cross sections. Resolved resonances to be screened are characterized by two types: (1) extremely wide resonances with natural widths much larger than both the corresponding Doppler width and the ultra-fine group width ($\Gamma_t \geq 50\Delta$ where Γ_t is the natural

width and Δ is the Doppler width) and (2) extremely week resonances belonging to the medium weight nuclides of low natural abundance or p-wave resonances of heavy nuclides of low natural abundance. These resonances normally have very little contribution to either the overall Doppler broadening effect or the self-shielding effect. This screening process yields significant reductions in MC^2-2 and RABANL execution times, especially for problems involving structural isotope resonances. In addition, screening out of resonances wider than a certain criterion is required for ultra-fine group calculations with analytic resonance integral based on the narrow resonance approximation.

The ETOE-2 code is able to treat single level, multilevel Breit-Wigner formulas or a multilevel Adler-Adler description. It also has capabilities to convert the Reich-Moore parameters into the multipole parameters or Adler-Adler parameters so that the cross section values at any energy and temperature can be represented as a linear combination of the Doppler-broadened line shape functions [29,30]. The ENDF/B data permit six secondary energy distribution laws for inelastic and (n,2n) scattering, whereas MC^2-2 permits only three of those. Thus, the ETOE-2 code generates a tabulated function if data are provided for any of the three laws which cannot be processed by MC^2-2.

The MC^2-2 code solves the neutron slowing down equation in the consistent P_1 or B_1 approximations and makes use of the extended transport approximation to account for high-order anisotropic scattering effects. The multigroup slowing-down equation based on ultra-fine group lethargy structure is solved above the resolved resonance energy, while the continuous slowing-down equation is solved for the resolved resonance range. In the continuous slowing-down formulation the moderating parameters are calculated using either Greuling-Goertzel (GG) [19] or improved GG algorithms. Only elastic scattering is treated continuously in the continuous slowing-down formulation. Inhomogeneous sources including fission, inelastic, and (n,2n) sources are represented in the ultra-fine group form.

Resolved and unresolved resonances are explicitly treated by the generalized J^* integral formulation based on the narrow resonance approximation including overlapping and Doppler broadening effects. The integration procedure is optimized by utilizing the asymptotic properties of the integrands and the general characteristics of the Gauss-Jacobi quadrature. This is archived by introducing a rational approximation of the variable of integration. For relatively week

resonances which represent a significant portion in practical calculations, the J^* integral is evaluated analytically. For the resolved energy range, algorithms are available for the multi-level Adler-Adler form, the single-level and multi-level Breit-Wigner forms, and the multipole representation of the Reich-Moore form. For the unresolved energy range, the algorithms provide an accurate estimate of the interference scattering influence as well as the overlap effect which accounts for the long-range correlation of levels described by Dyson [31].

The J^* integral method provides an efficient means of accounting for resonance effects in the continuous slowing-down formulation. In particular, the continuous slowing-down equations are solved for the asymptotic neutron slowing-down density ignoring narrow resonances. The resonance reaction rates are then computed using the flux resulting from the asymptotic slowing-down density attenuated by the absorption in higher energy resonances. The ultra-fine group flux derived from the attenuated slowing-down is used for generating broad group cross sections by the standard group collapsing method.

Inelastic and (n,2n) secondary energy distributions may be described by discrete levels, evaporation spectra, or tabulated functions in accordance with the ENDF/B specifications. Detailed angular distributions are used in calculating ultra-fine group P_0 and P_1 elastic scattering matrices for all isotopes. For light isotopes, an analytic integration over the sink group is combined with a detailed numerical integration over the source group. Heavy isotope transfer matrices are calculated in a semi-analytic manner.

For resolved resonance integral calculation, as aforementioned, the MC^2-2 code uses the narrow resonance approximation. An alternative RABANL option is also available to use the hyper-fine group integral transport calculation, providing a rigorous treatment of resolved resonance cross sections for use in the lower energy ranges for which the narrow resonance approximation is not valid. The RABANL module performs a hyper-fine-group slowing down calculation by dividing the resolved resonance Doppler width into a few groups. The hyper-fine group value for those ultra-fine group data are created by a simple linearlization algorithm. Inelastic and (n,2n) scattering sources, fission sources at energies above the upper limit of the RABANL energy range are treated as external sources, being supplied from the SRATES file [3] which is obtained from the ultra-fine group calculation. Options are also available for

inhomogeneous group-dependent sources, group-dependent buckling, and buckling search calculations. Figure 3.2 illustrates the calculation flow of the MC^2-2 code.

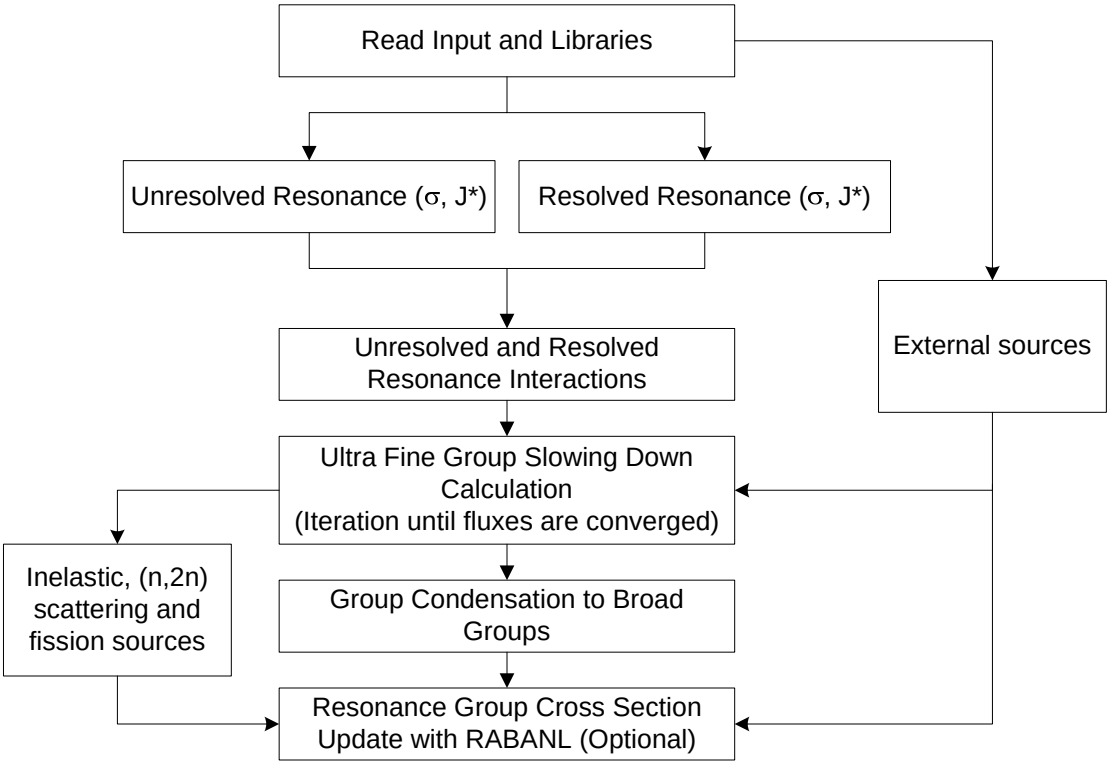

Figure 3.2 Generation of Problem-Specific Multigroup Cross Sections in MC^2-2.

3.2 Improvement Needs

The ETOE-2 code has been continually modified to process the ENDF/B-III, -VI, -V, and –VI files, which were released in 1972, 1974, 1978, and 1990, respectively. The resulting MC^2-2 libraries were extensively verified and validated up to the version V.2 of ENDF/B data, and applied successfully for fast reactor analysis. In late 1990s, significant modifications were made on the ETOE-2 code in order to process the ENDF/B-VI data by converting the Reich-Moore formalism to the multipole formalism [32]. However, only limited verification and validation studies were performed for the ENDF/B-VI libraries. As a result, the ENDF/B-V.2 libraries have been used preferably even now. To take full advantage of the improved nuclear data in recently

released ENDF/B-VII.0, the compatibility of the ETOE-2/MC^2-2 system with the new data representations needs to be tested thoroughly, and necessary modifications should be made.

From the programming point of view, the ETOE-2/MC^2-2 codes are old-fashioned. They were programmed in old versions of FORTRAN and contain many out-dated programming syntaxes, functions, and structures. The data and memory management schemes developed for the computer architectures in late 1970s and early 1980s [33] also make it difficult and inefficient to maintain and update the codes and to link them to other codes in the modern computing architecture and environment. It is therefore necessary to rewrite the codes in modern language standards for eventual coupling with UNIC and use in parallel computing environments.

In order to identify potential issues and improvement needs, the status of ETOE-2 and MC^2-2 codes was reviewed thoroughly, focused on enhancing the accuracy and efficiency. The identified improvement needs are as follows:

(1) The codes need to be rewritten in terms of memory structure and programming syntaxes using modern language tools (e.g., FORTRAN 90/95). It is very essential for the future coupling with the UNIC code, in particular in a parallel computing environment.

(2) Capabilities and functions to process the latest versions of ENDF/B files should be implemented and verified. Specifically, the codes should be able to handle the recently released ENDF/B-VII data which are reported to have many changes compared to the previous ENDF data. In particular, the algorithms for resolved resonance data treatment of converting the Reich-Moore parameters to the multipole representation, which were implemented based on the algorithms of the WHOOPER and WHOOPJR codes [29,30], need to be verified thoroughly. Detailed tests are also required of the algorithms to process other data such as unresolved resonances and fission spectrum distributions.

(3) In the ETOE-2 code, extremely week and wide resonances are screened out to enhance the computation efficiency and to minimize the error due to the narrow resonance approximation. The screening criteria which were developed based on the ENDF/B-V data need to be re-evaluated for the new ENDF/B data.

(4) In the MC^2-2 code, the slowing down equation is solved using two different methods: continuous slowing down theory method for the resolved resonance energy range and

multigroup method for above resolved resonance range. In the continuous slowing down theory method, the slowing down due to hydrogen and the higher order anisotropic scatterings are treated rather approximately. The main motivation to implement the continuous slowing down method was to save the computation memory and time, but the computing power and resources are no longer limiting factors in modern computing environments. Therefore, it appears to be desirable to eliminate the complexities in program and to enhance the accuracy by employing the multigroup formulation for the whole-energy range.

(5) In the RABANL module of MC^2-2, the anisotropic scattering is treated under the assumption that the broad group (the energy structure of the output data set) down-scattering is confined to a single energy group. Thus, higher order scattering matrices are not explicitly calculated. This assumption is only valid for analyzing the P_0 scattering cross sections for broad group structures ($\Delta u \geq 0.174$), and hence the higher-order equations need to be explicitly solved for more accurate estimation of anisotropic scattering cross sections.

(6) In RABANL, neutron sources due to inelastic and (n,2n) scattering reactions and fission reactions at the energies above the RABANL energy range are provided from the ultra-fine group calculation through the SRATE file. These ultra-fine group data are expanded to hyper-fine group values by a linearlization algorithm. To improve the accuracy, discrete-level and continuum inelastic reactions need to be considered explicitly in the hyper-fine group level.

(7) In MC^2-2, scattering sources due to inelastic and (n,2n) scattering are assumed to be isotropic. This assumption would be reasonable for practical reactor calculations, but the anisotropy of inelastic scattering reaction becomes non-negligible in the systems with very hard spectrum such as the LANL fast criticality assemblies. Therefore, the anisotropy of inelastic scattering needs to be taken into account.

(8) For the fast reactor system with a large amount of structure material, it is necessary to shield properly the resonance-like scattering cross sections of medium-weight nuclides such as Fe, Cr, Ni, Mn, Co, and Cu in the above resonance energy region, shown in Figure 3.3. It is normally required to use more than 8,000 groups in order to catch more than 90% of the self-shielding effect of these resonance-like scattering cross sections. In the current practice, the

shielded cross sections are prepared separately and incorporated into the smooth cross section library of MC^2-2 using the SHIELD program [34], which directly reads the ENDF file to reconstruct the detailed cross section curves and replaces all principle smooth cross sections by the shielded ones. To simplify the cross section generation scheme, it is desirable to incorporate this shielding calculation into the ETOE-2 and MC^2-2 calculations.

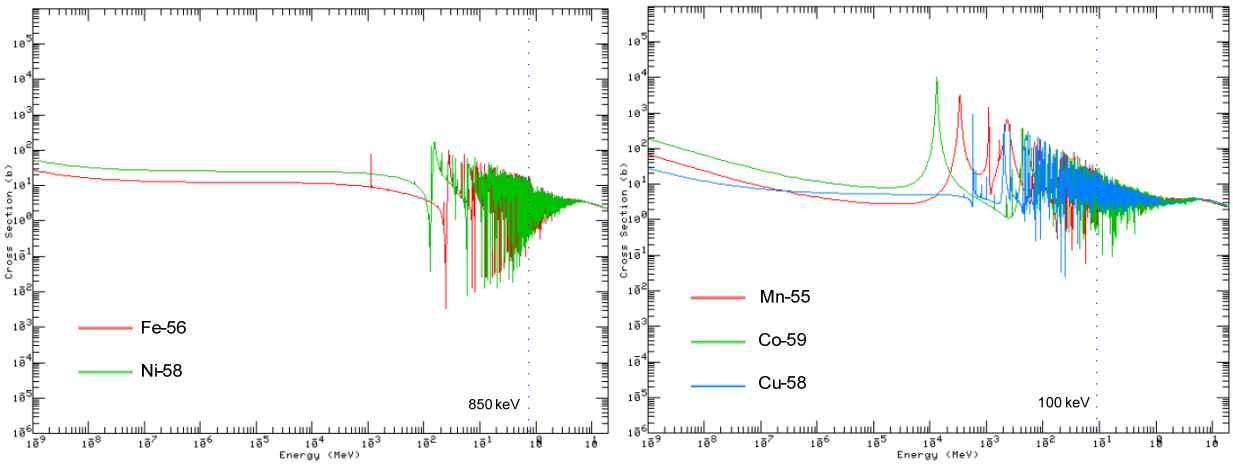

Figure 3.3 Total Cross Sections of Fe-56, Ni-58, Mn-55, Cu-58, and Co-59.

4. Status of ETOE-2/MC^2-2 Revision

To implement the needed improvements discussed in Section 3, work initiated on revising the ETOE-2/MC^2-2 codes. This year focus was on the required revision to process the recently released ENDF/B-VII.0 data**.** Conversion in FORTRAN 90/95 was also initiated for eventual coupling with UNIC and use in a parallel computing environment. At present, the ENDF/B-VII.0 data has been processed for major heavy and intermediate mass nuclides employed in sodium-cooled fast reactor. Preliminary tests of the ENDF/B-VII.0 libraries of MC^2-2 have also been performed using a set of fast critical benchmark problems.

In this section, modifications made on the selected ETOE-2/MC^2-2 system are summarized. The status of ENDF/B-VII.0 data processing and its initial verification and validation results are also presented. .

4.1 Code Updates

Since the library files generated by ETOE-2 are not composition dependent, the program need to be executed only when new fundamental data become available (e.g., each release of ENDF/B). Thus, when coupled with the neutron transport code, the ETOE-2 code will still remain standalone and the MC^2-2 code will be the main one to be coupled. Therefore, an initial focus of code conversion was put on the update of MC^2-2 in terms of memory structure and programming syntaxes.

Several subroutines and functions were also modified to process the ENDF/B-VII data properly. These include changes in unresolved and resolved resonance data processing, resolved resonance screening process, and fission spectra processing. Among the improvement needs discussed in Section 3.2, the items (4) to (8) remain as future works.

Code Structure

The MC^2-2 code is composed of multiple independent “executable” modules using a separate data management package (BPOINTR) subroutines and functions for retrieving and storing data. Thus, modules communicate each other through binary files by reading and writing

data on the files at the beginning and end of each module. Data arrays and their addresses are refreshed and set up at the beginning of each module. The main storage of data is a sequential, one-dimensional double-precision real container which is shared with single-precision real, double-sized character, and single-precision integer arrays. These data and memory management schemes were the best solution to manage memories and data one-time, but the separate executable modules and the BPOINTR-type data management make it difficult and inefficient to update or couple the MC^2-2 code with other code systems. Therefore it was decided to eliminate these out-dated modular programming and data management schemes.

Major changes in the MC^2-2 code made this year in terms of the programming level are as follows:

- All executable modules were merged to provide one executable and successfully compiled using FORTRAN 90 compilers on different platforms such as Sun Solaris and PC Window.
- The memory structure with old-fashioned common blocks was changed to FORTRAN 90 based modules.
- All the BPOINTR functions and subroutines for handling memory and data were replaced with FORTRAN 90 based routines.

In the next step, the code will be reshaped by replacing the huge one-dimensional array container by separate multi-dimensional arrays and removing unnecessary read/write routines and interface files for the data transfer between functional modules.

Unresolved Resonances

In the ENDF/B data, the flag LSSF is used to specify the different procedures for processing the unresolved resonance cross sections. Per the ENDF/B-VI formats manual [35], if LSSF is set equal to zero, File 3 contains partial background cross sections to be added to the average unresolved cross sections calculated from the parameters in File 2. If LSSF is set to one, File 3 represents the entire dilute unresolved cross section and no File 2 contribution is to be added to it. In this case, the parameters in File 2 are used to compute the self-shielding factors

that may be applied to the File 3 values. The option with LSSF = 1 is a new feature for ENDF/B-VI and therefore the relevant MC^2-2 routines have been updated and verified.

In the MC^2-2 code, when LSSF is equal to zero, the additive terms for unresolved total, fission, and capture cross sections are used to compute the additive term for the unresolved elastic scattering cross section as:

$$\Delta\sigma_{es}^{u} = \Delta\sigma_{t}^{u} - \Delta\sigma_{c}^{u} - \Delta\sigma_{f}^{u}, \tag{4.1}$$

where $\Delta\sigma_{es}^{u}$, $\Delta\sigma_{t}^{u}$, $\Delta\sigma_{c}^{u}$, and $\Delta\sigma_{f}^{u}$ are the additive terms for unresolved elastic scattering, total, capture, and fission cross sections, respectively. When LSSF is equal to one, the unresolved cross sections are directly derived by multiplying the shielding factors and accordingly the unresolved elastic scattering cross section is computed as:

$$\sigma_{es}^{u} = \sigma_{t}^{u} - \sigma_{c}^{u} - \sigma_{f}^{u} - \sum_{os \neq es} \sigma_{os}, \tag{4.2}$$

where $\sigma_{t}^{u} = \sigma_{t} \cdot f_{t}^{u}$, $\sigma_{c}^{u} = \sigma_{c} \cdot f_{c}^{u}$, $\sigma_{f}^{u} = \sigma_{f} \cdot f_{f}^{u}$,

σ_{t}, σ_{c}, σ_{f} = smooth total, capture, and fission cross sections,

f_{t}^{u}, f_{c}^{u}, f_{f}^{u} = shielding factors for unresolved total, capture, and fission cross sections,

σ_{os} = other types of scattering cross sections.

Since the total cross section includes all types of scattering cross sections, other types of scattering cross sections (inelastic scattering cross sections in the unresolved resonance energy region) as well as capture and fission cross sections should be subtracted from the total cross section to obtain the elastic scattering cross section only. For example, the inelastic scattering cross sections of U-238 have a contribution of about 6% to the total cross section around the upper energy limit of the unresolved resonance regions (the unresolved resonance energy range of U-238 is 20~150 keV).

Only the single-level Breit-Wigner formalism is allowed for unresolved resonance parameters. In addition, there are three ENDF formats available for specifying the energy-dependence of the parameters using the flags LFW and LRF: (1) LFW=0 (fission width is not

given) and LRF=1 (all parameters are energy-independent), (2) LFW=1 (fission width is given) and LRF=1 (only fission widths are energy dependent and the rest are energy-independent), and (3) LRF=2 (all energy-dependent parameters) which does not depend on LFW. Formats 1 and 2 can be represented with Format 3. The current version of ETOE-2 handles only Format 3 which is used in ENDF/B-VII.0 for most nuclides except for Pu-238. Therefore, the unresolved resonance data in the ENDF/B file of Pu-238 were converted to Format 3 prior to the ETOE-2 processing. Eventually, the code will be changed to be able to treat the other formats.

Resolved Resonances

In the ETOE-2/MC^2-2 code suite, the R matrix parameters in the Reich-Moore formalism are converted to the multipole parameters so that both the rigor of the Reich-Moore cross sections and the desirable features (the cross section value at any energy and temperature can be represented as a linear combination of the Doppler-broadened line shape functions) of the traditional formalisms can be preserved. Cross sections in the Reich-Moore formalism can be expressed using the rigorous pole representation as [29]:

$$\sigma_x = \frac{1}{E}\sum_{l,J}\sum_{\lambda=1}^{N}\sum_{j=1}^{2(l+1)} \mathrm{Re}\left[R_{l,J,j,\lambda}^{(x)} \cdot \frac{(-i)}{p_\lambda^{(j)*} - \sqrt{E}} \right], \tag{4.3}$$

where $p_\lambda^{(j)*}$ = pole for level λ and complex conjugate pair j,

$R_{l,J.j,\lambda}^{(x)}$ = residue for state ℓ, spin J, complex conjugate pair j, and level λ including the phase shift factor $\exp(-i2\phi_l)$ for $x \in R$,

x = reaction type,

J = spin,

l = angular momentum state,

N = total number of Reich-Moore resonances.

For the s-wave, the rigorous pole representation and the traditional formalism consist of an identical number of terms with the same functional form in the momentum domain. In particular, the Adler-Alder formalism for the s-wave can be considered as a special case of the

former when $p_\lambda^{(1)} = -p_\lambda^{(2)}$ and $R_{l,J,1,\lambda}^{(x)} = R_{l,J,2,\lambda}^{(x)}$. In this regard, Eq. (4.3) can be simplified by regrouping the pole terms as:

$$\sigma_x = \frac{1}{E}\sum_l \ \mathrm{Re}\left\{\sum_J \ \sum_{\lambda=1}^{N} \left(R_{l,J,1,\lambda}^{(x)} \cdot \frac{2(-i)\sqrt{E}}{\left[p_\lambda^{(1)*}\right]^2 - E} \right) + s_l^{(x)}\left(\sqrt{E}\right) + q_l^{(x)}\left(\sqrt{E}\right)\cdot \delta_l \right\}, \qquad (4.4)$$

where $s_l^{(x)}\left(\sqrt{E}\right) = \sum_J \ \sum_{\lambda=1}^{N} \left\{ \frac{R_{l,J,2,\lambda}^{(x)}(-i)}{p_\lambda^{(2)*} - \sqrt{E}} + \frac{R_{l,J,1,\lambda}^{(x)}(-i)}{p_\lambda^{(1)*} + \sqrt{E}} \right\}$,

$q_\ell^{(x)}\left(\sqrt{E}\right)$ = contributions of the smooth terms consisting of the sum of the pole terms attributed to $j \notin 1, 2$ for a given l,

$$\delta_l = \begin{cases} 0, \ if \ \ l = 0 \\ 1, \ \ if \ \ l > 0. \end{cases}$$

Thus, the rigorous pole representation can be viewed as a combination of a fluctuating term consisting of N poles with $\mathrm{Re}\, p_\lambda^{(1)} > 0$ and two non-fluctuating terms attributed to the tails of outlying poles with negative real component ($s_l^{(x)}$) and the poles with extremely large width for $l > 0$ states ($q_l^{(x)}$), respectively. The smooth behavior of the non-fluctuating components in the effective range of interest can be reproduced using simpler functions rather than the computation of numerous pole terms. Therefore, the terms of $s_l^{(x)}$ and $q_l^{(x)}$ are expressed in the form of pole expansion with a few number of pseudo poles (mostly 3 pseudo poles are sufficient). For s-waves, the spacing of the poles in momentum space is reasonably distant as the result of Wigner repulsion. Therefore, the computation of multipole parameters for the s-wave resonances is trivial. For higher l states, however, the poles in question generally consist of $2N$ s-wavelike poles with distant spacing and $2l \cdot N$ poles with extremely closely spaced regardless of how well separated the input Reich-Moore resonances are.

The ETOE-2 code is using the same routines as in WHOPPER and WHOPJR codes [29,30] in which the poles are determined using the Newton-Raphson algorithm. The pseudo poles are tagged as well as the poles for resonances outside the lower (E_l) and upper (E_u) boundaries of the resolved region. In MC^2-2, the contribution of the pseudo poles is calculated and added to the smooth cross sections prior to the resonance integral calculation. In addition,

the poles for the resonances outside the resolved region (e.g., 29 out of 3343 resonances in U-238 of ENDF/B-VII.0) are treated as pseudo poles so that the resolved resonance integral calculation can be performed within a given energy domain, $E_l \le E \le E_u$.

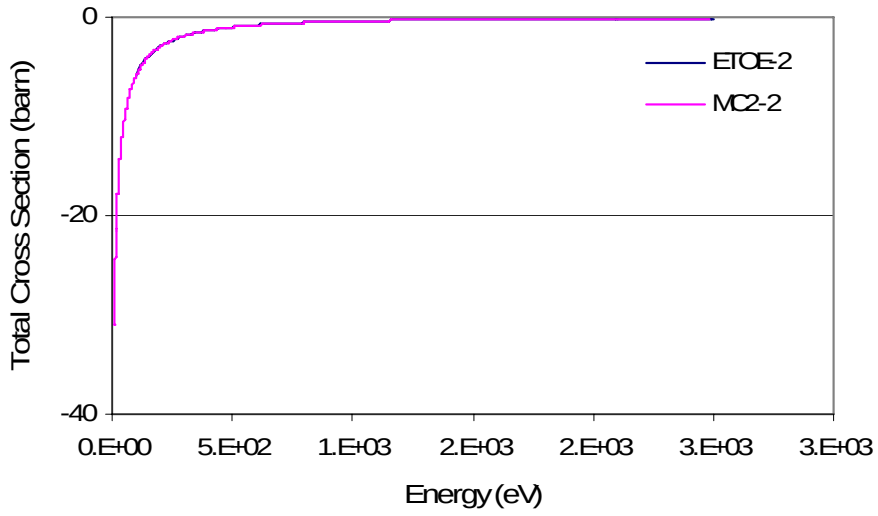

Figure 4.1 Contribution of Pseudo Poles to Total Cross Section of Pu-239.

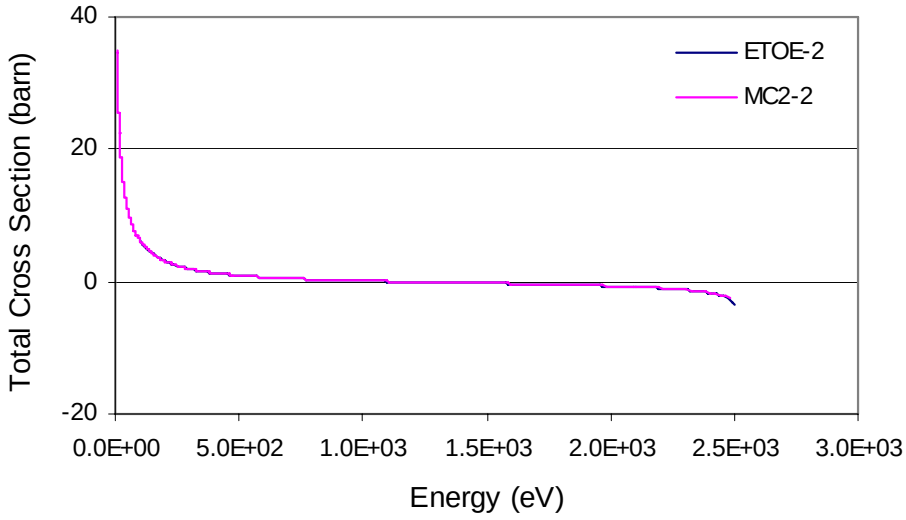

Figure 4.2 Contribution of Out-Range Poles to Total Cross Section of Pu-239.

Figure 4.1 shows the smooth behavior of the non-fluctuating components represented by pseudo poles in Pu-239. The tails of outlying poles with negative real components die out

gradually with increasing energy. Figure 4.2 presents the contributions from the out-range poles in Pu-239. As expected, the magnitude of contributions is decreasing with a distance from both energy boundaries. As can be seen in the figures, the outlying pole and out-range pole contributions from ETOE-2 are confirmed to be very well reproduced in MC^2-2.

Unlike other nuclides, the resolved resonance energy data of Pu-239 in ENDF File 2 are divided into three independent sections: 0 ~ 1 keV (7 out-range ones out of 405 resonances), 1 ~ 2 keV (6 out-range ones out of 441 resonances), and 2 ~ 2.5 keV (6 out-range ones out of 224 resonances). The out-range fictitious resonance parameters take into account the contribution of all the external truncated resonances in such a way that no total, scattering, fission, and capture smooth files are needed in the corresponding energy ranges for the reproduction of the cross sections. However, the contributions of out-range parameters are limited to each separate section. Currently, the ETOE-2/MC^2-2 code suite is not able to handle more than one section along with the multipole option. Therefore, the Reich-Moore parameters of Pu-239 were transformed to the Adler-Adler formalism which is acceptable for Pu-239 s-wave resonances. In future, the codes will be able to process multiple sections of Reich-Moore parameters with the multipole option.

Screening Criteria

As mentioned in Section 3, the ETOE-2 code preprocesses the resonance data by screening out wide resonances (which are temperature independent and well represented by the ultra-fine group structure of MC^2-2) and extremely narrow resonances (which do not contribute significantly to the self-shielding or Doppler effects). The resonance treatment in MC^2-2 assumes that the effects of an individual resonance are confined to a narrow energy range surrounding the resonance peak, based on the narrow resonance approximation. In other words, the entire resonance contribution to the reaction rates occurs in the single ultra-fine group containing the resonance peak. As a result, although the narrow resonance treatment allows a refined evaluation of the Doppler broadened energy self-shielding effects, the effect of the resonance tails on neighboring ultra-fine groups is neglected. This causes the over-prediction of the cross sections at energies below the resonance peak and the under-prediction at energies above the resonance peak, as illustrated in Figure 4.3.

The resonance screening algorithm in ETOE-2 should determine which resonances require the narrow resonance treatment and which can be better represented in the smooth ultra-fine group cross sections. In the smooth data, the energy dependence of the resonance cross section including the extended tail effect is explicitly modeled, although an infinite dilution resonance spectrum is applied. Therefore, the resonance screening process is a tradeoff between the accurate treatment of resonance self-shielding and the limitation of the narrow resonance approximation.

One of the resonance screening processes adopted in ETOE-2 is to preprocess the resonances which have significantly extended resonance tail effects with $\Gamma_t / \Delta >> 1$, where Γ_t and Δ are the total line width and the Doppler line width, $(4kTE/A)^{1/2}$, respectively. Resonance scattering cross sections are formulated as:

$$\sigma_s = 4\pi\lambda^2 \sum \sum \frac{\Gamma_{nR}}{\Gamma_{tR}} \left[\cos 2\phi_l \psi + \sin 2\phi_l \chi\right], \tag{4.5}$$

where $\psi = \dfrac{1}{1+x^2}$ (symmetric Doppler broadened line shape function),

$\chi = \dfrac{2x}{1+x^2}$ (asymmetric Doppler broadened line shape function) with $x = \dfrac{E - E_R}{\Gamma_t / 2}$,

ϕ_l = the hard-sphere phase shift factor,

E_r = the resonance peak energy.

The integral of the line shape function for the ultra-fine group neighboring the resonance origin and all subsequent groups up to the maximum scattering range becomes [36]

$$C_1 = \frac{1}{(x_2 - x_1)} \int_{x_1}^{x_2} \frac{1}{1+x^2} dx = \frac{\tan^{-1} x_2 - \tan^{-1} x_1}{(x_2 - x_1)}, \tag{4.6}$$

$$C_2 = \frac{1}{(x_2 - x_1)} \int_{x_1}^{x_2} \frac{2x}{1+x^2} dx = \frac{\ln\left[(1+x_2^2)/(1+x_1^2)\right]}{(x_2 - x_1)},$$

where $x_1 = E_R(1 - e^{-\Delta u})/(\Gamma_t / 2)$,

$x_2 = E_R(1-e^{-N\cdot\Delta u})/(\Gamma_t/2)$ with $N = -\text{int}[\ln\alpha^2/\Delta u]$,

$\alpha = (A-1)/(A+1)$,

Δu = ultra-fine group lethargy interval (=1/120),

A = atomic mass,

C_1, C_2 = symmetric and asymmetric terms, respectively.

The test indices for importance of a resonance to the scattering cross section are defined for symmetric and asymmetric components as:

$$T_1 = C_1 \cdot \cos(2\phi_l) \cdot \frac{\sigma_0}{\sigma_p}, \tag{4.7}$$

$$T_2 = C_2 \cdot \sin(2\phi_l) \cdot \frac{\sigma_0}{\sigma_p},$$

where σ_0 is the peak cross section for the resonance, σ_p is the hard sphere potential scattering cross section and ϕ_l is the phase shift factor.

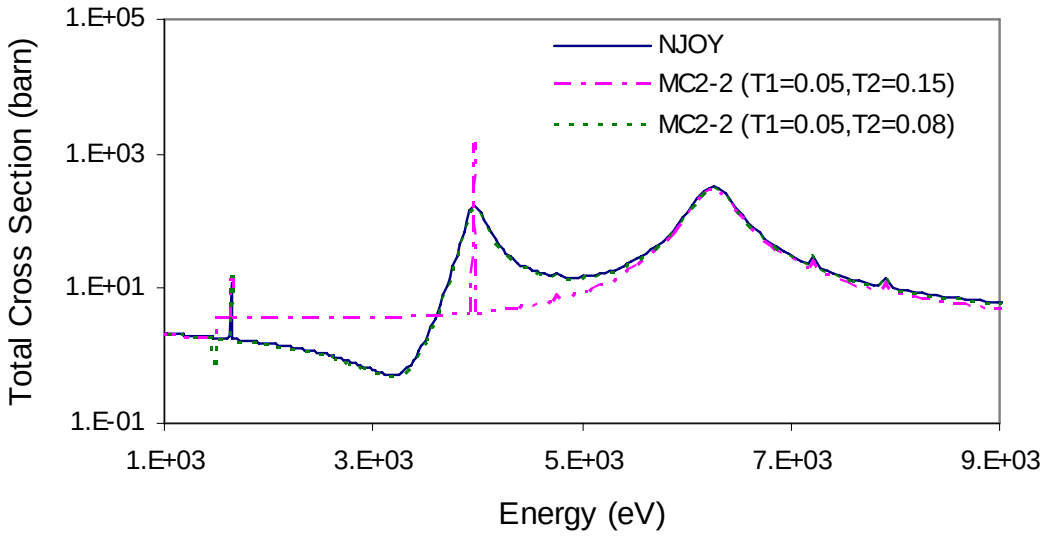

Figure 4.3 Total Cross Sections of Fe-57 from NJOY and MC^2-2 with Change of Screening Test Criteria.

For most nuclides, the resonances with significantly extended tail effects have been successfully preprocessed with the criteria of $T_1 = 0.05$ and $T_2 = 0.15$. However, it was found that these criteria are not adequate for a few medium-weight isotopes such as Fe-57 and Cr-53, as shown in Figure 4.3. Thus, the T_2 value was reduced to 0.08 for those isotopes.

Fission Neutron Spectrum

With the evolution of ENDF/B data, the fission neutron energy distribution data have been upgraded from a single set of table to multiple tables as a function of incident neutron energy, for many nuclides (Th-232, U-234, U-235, U-238, Pu-241, etc.). Table 4.1 shows changes in the table format (File 5, MT=18) for fission energy distributions over ENDF files.

Table 4.1 Change of Secondary Particle Energy Distribution Data Format in Major Actinides.

Nuclide	Energy Distribution of Secondary Particle (File 5, MT=18)		
	ENDF/B-V.2	ENDF/B-VI.8	ENDF/B-VII.0
Th-232	S	S	M
U-233	S	S	S
U-234	S	S	M
U-235	S	M	M
U-236	S	S	S
U-238	S	S	M
Pu-238	S	S	S
Pu-239	M	M	M
Pu-240	S	S	S
Pu-241	S	S	M
Pu-242	S	S	S

* S: Single data set, M: Multiple data set

Currently, the MC^2-2 code does not allow the incident neutron energy dependent fission neutron spectrum. Thus, the ETOE-2 code generates the fission neutron spectrum for a given effective fission spectrum energy input (e.g., 3 MeV for U-238, 500 keV for Pu-239, and 300 keV for U-235). On the other hand, using a given weighting function or the flux solution from the flux calculator, the NJOY code determines the fission neutron spectrum dependent on the incident neutron energy as:

$$\chi(E) = \frac{\int_0^\infty \chi(E' \to E) \nu\sigma_f(E')\phi(E')\,dE'}{\int_0^\infty \nu\sigma_f(E')\phi(E')\,dE'}, \tag{4.8}$$

where E' is an incident neutron energy.

Multigroup fission spectra depend on the flux in the system of interest, and the variation of fission spectrum increases with increasing incident neutron energy. As a result, the incident neutron energy-independent approximation of fission spectrum of ETOE-2 determined with a given effective incident neutron energy would introduce non-negligible errors for fast reactor analysis. For example, by comparing fission spectrum distributions of U-238 obtained from NJOY and MC^2-2 based on ENDF/B-VII.0 data, it was found that the broad-group fission spectra from the two codes were different by more than ±3%. It is noted that for the NJOY calculation the fast spectrum weighting function (IWT=8 in which Maxwellian, 1/E, fission and fusion spectrum distributions are used for thermal, intermediate, fast energy regions, respectively) was used.

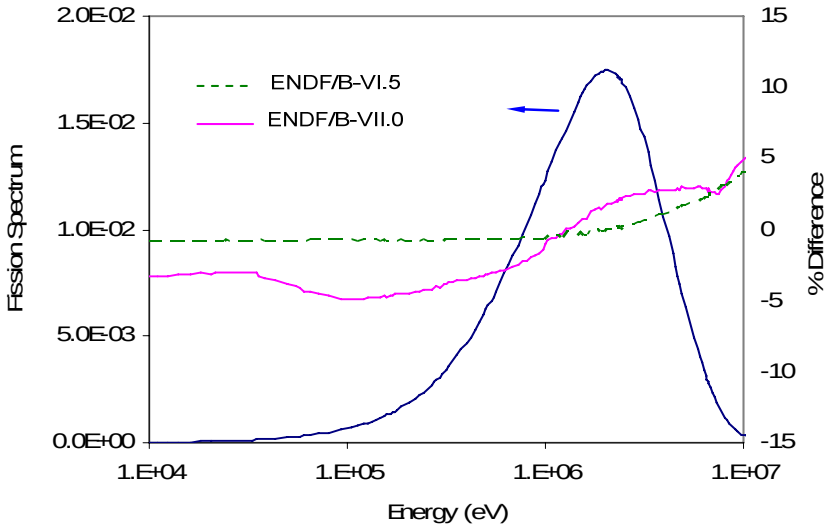

Figure 4.4 Comparison of 230-group Fission Spectra of U-238 from NJOY and MC^2-2 (ENDF/B-VI.5 and ENDF/B-VII.0).

Figure 4.4 compares the 230-group fission spectra of U-238 obtained from NJOY and MC^2-2 calculations based on the ENDF/B-VI and ENDF/B-VII data. As shown in Table 4.1, the fission neutron spectrum of U-238 is presented in multiple tables as a function of incident

neutron energy in the ENDF/B-VII.0 data, while it was given as a single table in the ENDF/B-VI data. It can be seen that the fission spectra of NJOY and MC^2-2 based on the ENDF/B-VI data agree well each other within less than ~1%, except for very high energy range. On the other hand, those based on the ENDF/B-VII data show significantly larger differences over the energy range of interest. This suggests that the ETOE-2 and MC^2-2 codes should be updated to be able to handle multiple sets of fission neutron energy distributions as a function of incident neutron energy.

Resonance-like Cross Sections

As discussed in Section 3, the resonance-like scattering cross sections of medium-weight nuclides in the above resonance energy region should be shielded for a fast reactor system with a large amount of structure material. Currently, the shielded cross sections are prepared separately and incorporated into the smooth cross section library of MC^2-2 using the SHIELD program [34]. Since those resonance-like cross sections are not affected by the temperature change, however, they can be self-shielded using the pre-calculated shielding factors as a function of background cross section only. The shielding factor table can easily be generated from the NJOY code or the SHIELD program with minor modification.

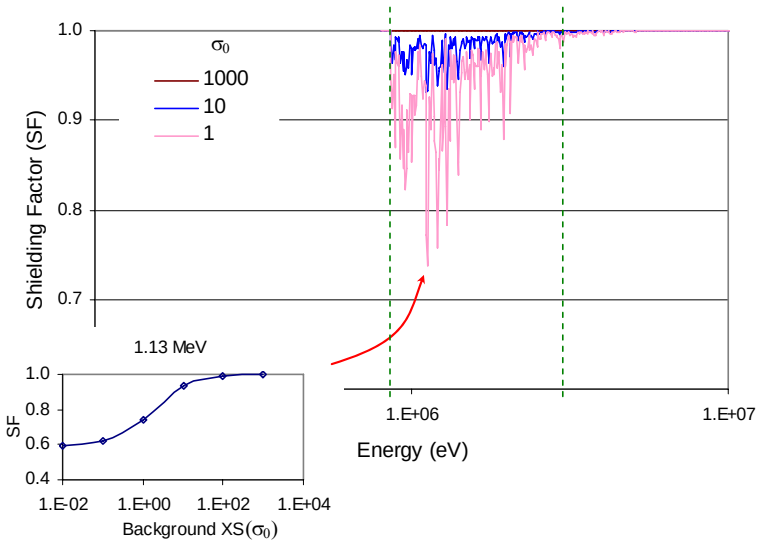

Figure 4.5 Shielding Factors (2082 groups) of Fe-56 Total Cross Sections above the Resonance Energy Range.

Figure 4.5 shows the 2082-group shielding factors for total cross sections of Fe-56 with different background cross sections. As can be seen, the shielding factors of Fe-56 (the upper energy limit of its resonance is 0.85 MeV) are effective in the energy range between 0.85 and 3 MeV: e.g., a typical background cross section of Fe-56 for the energy range is ~10 barns. In order to implement the shielding factor table in the MC^2-2 code, the ultra-fine-group cross sections of a specific isotope will be adjusted depending on its background cross section.

4.2 Processing of ENDF/B-VII.0 Data

Characteristics of ENDF/B-VII.0

The ENDF/B-VII.0 files released in December 2006 contain the primary data for reactions with incident neutrons, protons, and photons on almost 400 isotopes, based on experimental data and theory predictions. The principal advances over the previous ENDF/B-VI library are as follows: (1) New cross sections for U, Pu, Th, Np and Am actinide isotopes with improved performance in integral validation criticality and neutron transmission benchmark tests; (2) More precise standard cross sections for neutron reactions on H, Li-6, B-10, Au and for U-235 and U-238 fissions; (3) Improved thermal neutron scattering; (4) An extensive set of neutron cross sections on fission products; (5) A large suite of photonuclear reactions; (6) Extension of many neutron- and proton-induced evaluations up to 150 MeV; (7) Many new light nucleus neutron and proton reactions; (8) Post-fission beta-delayed photon decay spectra; (9) New radioactive decay data; (10) New methods for uncertainties and covariance, together with covariance evaluations for some sample cases; (11) New actinide fission energy deposition.

After extensive validation studies, it has been reported that major improvements in ENDF/B-VII.0 are: (a) The long-standing underprediction of low enriched uranium thermal assemblies is removed; (b) The U-238 and Pb-208 reflector biases in fast systems are largely removed; (c) The good agreement of ENDF/B-VI.8 data for simulations of high-enriched uranium thermal assemblies is preserved; (d) The underprediction of fast criticality of U-233, U-235, and Pu-239 assemblies is removed; (e) The intermediate spectrum critical assemblies are predicted more accurately.

Processing of ENDF/B-VII.0 using ETOE-2

Using the updated ETOE-2 code, the recently released ENDF/B-VII.0 data have been processed. Due to the code updates discussed in the previous section, all selected nuclides except Pu-239 and Th-232 have successfully been processed without any functional problems. Table A.1 in Appendix A shows the number of resonances for each resonant nuclide that were survived from the screening process of ETOE-2. For Pu-239 and Th-232, alternative options have been applied.

The resolved resonance data (MT=151 in File 2) of Pu-239 are divided into three sections (0 eV ~ 1 keV, 1 ~ 2 keV, and 2 ~ 2.5 keV) including Reich-Moore parameters. The current version of ETOE-2 cannot process data in more than one region with the multipole representation option. Thus, the Reich-Moore parameters were converted to the Adler-Adler representation which appears to be acceptable for Pu-239 resonances. Unlike the other nuclides and its previous ENDF/B data, the fission energy distribution data (MT=18) of Th-232 belong to File 6 in ENDF/B-VII.0. Thus, the fission spectrum distribution data of Th-232 was obtained from NJOY calculation. The ETOE-2 code will be updated for those problems in future.

As an initial attempt to check whether the ENDF/B.VII.0 data was processed correctly, the MC^2-2 libraries generated from ENDF/B-VII.0 data were tested by inter-comparison of twenty-one group infinite dilute total cross sections obtained from MC^2-2, VIM [37], and NJOY (version 99.161) calculations at a temperature of 300 K. The 21-group structure is shown in Table 4.2. In order to make an infinite dilute condition in the MC^2-2 and VIM calculations, a large amount ($>10^5$ neutrons/cm^3) of oxygen (almost a constant scattering cross section of ~4 barns up to 300 keV) was added to the compositions having a very small amount (10^{-4} neutrons/cm^3) of each nuclide of interest. In NJOY calculations, the fast reactor weighting function (IWT=8) was used, although it might be quite different from the MC^2-2 or VIM spectrum at the very high energy range because of oxygen resonances. Therefore, total cross sections from NJOY for the highest three groups might not be comparable with those from other codes. Figure 4.6 shows the difference of spectra between NJOY and MC^2-2. As expected, both MC^2-2 and NJOY spectra show the asymptotic 1/E behavior below ~300 keV.

Table 4.2 Structure of 21 Energy Groups.

Group	Upper Energy (eV)	Group	Upper Energy (eV)
1	1.417 E+7	12	4.087 E+4
2	6.065 E+6	13	2.500 E+4
3	3.679 E+6	14	1.503 E+4
4	2.231 E+6	15	1.000 E+4
5	1.353 E+6	16	5.531 E+3
6	8.209 E+5	17	3.355 E+3
7	4.979 E+5	18	2.500 E+3
8	3.020 E+5	19	1.234 E+3
9	1.490 E+5	20	4.540 E+2
10	1.111 E+5	21	6.144 E+1
11	6.738 E+4	Lower Limit	0.414

The RABANL option of MC^2-2 was additionally used to check if cross sections are correctly reconstructed in the low energy region where the narrow resonance approximation is not valid. For VIM Monte Carlo calculations, the cross section libraries for ENDF/B-VII beta 2 were used, which are the latest version of VIM libraries available for ENDF/B-VII and are reported to have minor differences from ENDF/B-VII.0 in most nuclides. One-hundred million neutron histories were used for cross section tallies, resulting that the standard deviations of VIM total cross sections were less than 0.4%.

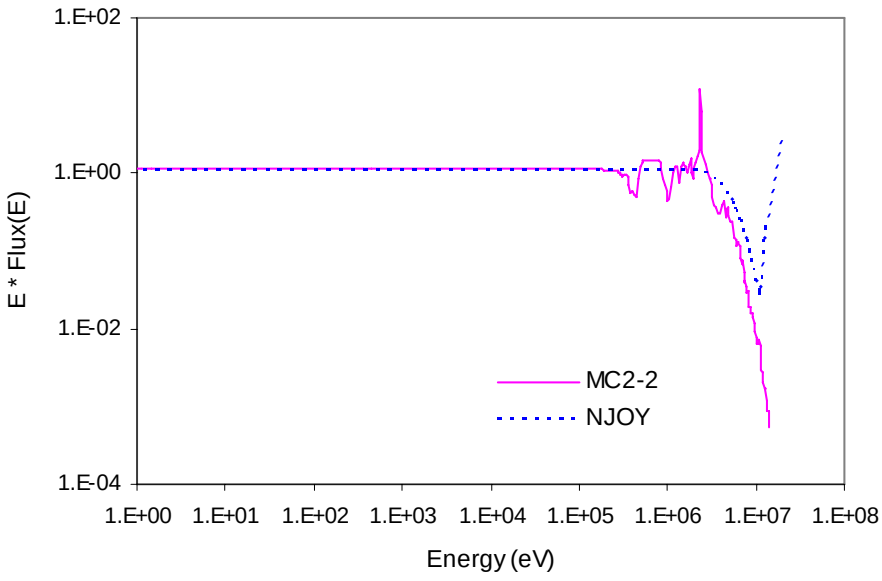

Figure 4.6 Neutron Spectra Used for Infinite Dilute Cross Section Generation in NJOY and MC^2-2.

The resulting 21-group cross sections of each isotope are compared in Tables A.2 through A.23 in Appendix A. It can be seen that infinite dilute total cross sections of ETOE-2/MC^2-2 agree very well with VIM or NJOY cross sections for most of all nuclides. In several nuclides such as U-234 (Group 10), Np-237, Pu-238 (unresolved resonance region), Pu-240 (Groups 11 and 12), molybdenum, and zirconium, the MC^2-2 cross sections are noticeably different from VIM cross sections, even though they are in very good agreements with NJOY cross sections. It is considered that the VIM cross section libraries of these isotopes have not been prepared with the latest release of ENDF/B-VII.

On the other hand, it is observed that the total cross sections of MC^2-2 are underestimated by up to 6% around the upper limit of the resolved resonance range for some actinides, compared to the VIM or NJOY cross sections: -4% for U-235 (group 18), -6% for U-238 (groups 13 ~ 14), and -2% for Pu-239 (group 18), for which the resolved resonance upper energy limits are 2.25 keV, 20 keV, and 2.5 keV, respectively. As mentioned before, the Reich-Moore parameters of the resolved resonance cross sections were converted to the mulitipole parameters for U-235 and U-238 and to the Adler-Adler parameters for Pu-239. Preliminary investigation showed that multipole, pseudo, and out-range poles generated in ETOE-2 are correct and their contributions are well reproduced in MC^2-2. To identify the reason for these discrepancies, further investigation needs to be performed.

The total cross sections of Ni-60 from MC^2-2 agreed fairly well with those of VIM or NJOY, except for group 17 (3.4 ~ 5.5 keV) where the difference is as large as about 16%. Thus, further investigation was performed by comparing more detailed group cross sections. As indicated in Figure 4.7, the group 17 corresponds to the tail part of the wide resonance at 12.5 keV, and in this energy interval, the average total cross section is as low as about 0.07 barns. Detailed comparison indicated that the difference had nothing to do with the screening process and could be attributed to the resolution of energy grids. The influence of this cross section would not be large in the resonance self-shielding.

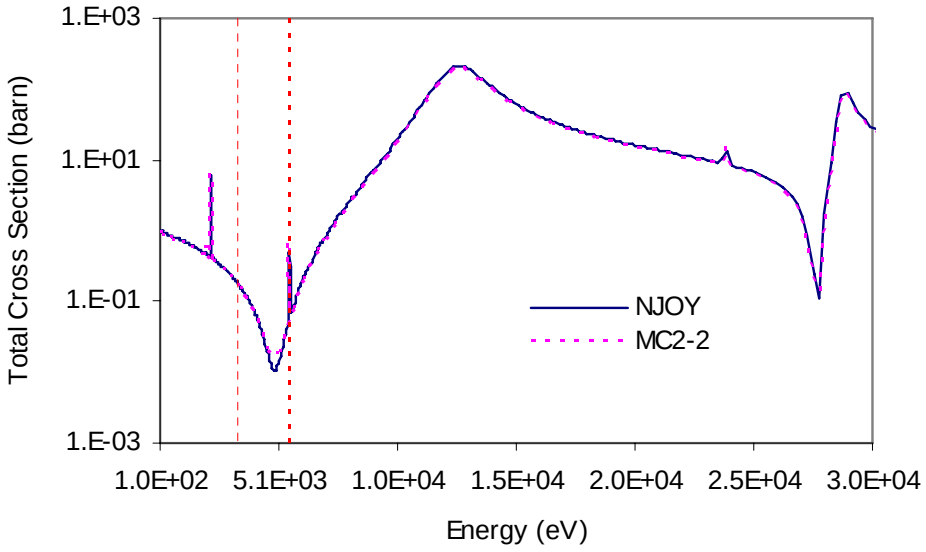

Figure 4.7 Total Cross Sections of Ni-60 from NJOY and MC^2-2.

4.3 Initial Verification and Validation

For initial verification and validation of the ENDF/B-VII.0 libraries of MC^2-2, a set of fast critical benchmark problems were analyzed, including eight LANL fast critical assemblies [7], two ANL ZPR fast critical assembles [7], and six ZPPR-21 critical assemblies [8-10]. The TWODANT [38] calculations were performed with the multigroup cross section sets obtained from MC^2-2 calculations. For comparison, MCNP [38] Monte Carlo calculations were also performed.

For deterministic TWODANT calculations, 230-group cross sections were generated for each distinct material zone with consistent P_N corrections. In MC^2-2 calculations, the critical buckling search option was used for a fuel zone, and a fixed source calculation was performed for a non-fuel zone using the leakage spectrum of an adjacent zone. For the cases with a large amount of iron, the resonance-like iron cross sections above the resonance energy range were shielded with additional hyper-fine-group calculations. The TWODANT calculations were performed with an angular quadrature of S_{24} and an anisotropic scattering order of P_5.

Table 4.3 compares the multiplication factors obtained from TWODANT and MCNP calculations. As can be seen, the TWODANT results agree well with MCNP [39] solutions (MCNP4C for ZPPR-21 and MCNP5 for the others) within ~0.25% Δρ, except for three cases (Godiva, Jezebel-240, and Jezebel-23). Relative to the MCNP solution, the TWODANT result overestimates the multiplication factor by 0.22 ~ 0.35% Δρ for the small systems without structural materials (a sphere geometry with less than 24 cm in diameter), while it shows better agreement for the big systems (Big-10, ZPR-6, and ZPPR-21) which have relatively softer spectrum. The spectra of Jezebel, Godiva, Flattop, Big-10, and ZPR-67 are compared in Figure 4.8. Among those systems, the Jezebel system is the hardest and the ZPR-67 system is the softest in spectrum.

Table 4.3 Comparison of Multiplication Factors for Fast Critical Systems.

Assembly	MCNP ± pcm	TWODANT Δρ, pcm	Assembly	MCNP ± pcm	TWODANT Δρ, pcm
Flattop-25	1.00212 ± 35	227	ZPR6-6A	0.99609 ± 23	22
Flattop-Pu	1.00072 ± 34	235	ZPR6-7	0.98671 ± 22	-126
Flattop-23	0.99921 ± 34	257	ZPPR-21A	0.99869 ± 20	-153
Godiva	0.99996 ± 32	350	ZPPR-21B	0.99293 ± 20	75
Jezebel-240	0.99944 ± 31	300	ZPPR-21C	0.99923 ± 18	-25
Jezebel-23	1.00007 ± 31	279	ZPPR-21D	1.00345 ± 20	253
Jezebel	1.00028 ± 30	216	ZPPR-21E	1.00485 ± 20	184
Big-10	0.99513 ± 19	-57	ZPPR-21F	1.00612 ± 20	11

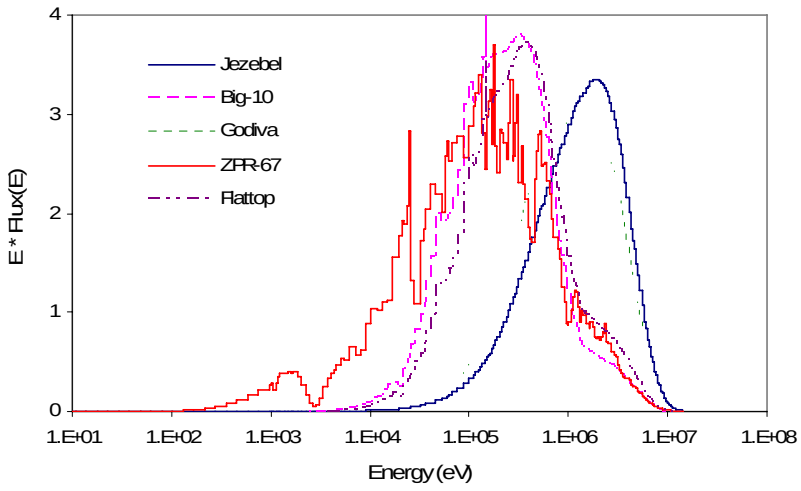

Figure 4.8 Neutron Spectra for LANL and ANL Fast Critical Systems.

Comparisons of measured and calculated fission reaction rate ratios of the Godiva and Jezebel assemblies are presented in Table 4.5. The TWODANT results agree well with the measured values within 2.7%. These results are comparable to those obtained with the previous ENDF data [32].

Table 4.4 Comparison of Measured and Calculated Fission Reaction Rate Ratios.

Isotope	Godiva		Jezebel	
	Experiment	TWODANT C/E ratio*	Experiment	TWODANT C/E ratio*
$\sigma_f^{U238}/\sigma_f^{U235}$	0.165 ± 0.002	0.973 ± 0.011	0.214 ± 0.002	0.978 ± 0.011
$\sigma_f^{U233}/\sigma_f^{U235}$	1.59 ± 0.03	0.987 ± 0.019	1.578 ± 0.027	0.987 ± 0.017
$\sigma_f^{Np237}/\sigma_f^{U235}$	0.837 ± 0.013	1.006 ± 0.015	0.962 ± 0.016	1.018 ± 0.016
$\sigma_f^{Pu239}/\sigma_f^{U235}$	1.402 ± 0.025	0.989 ± 0.018	1.448 ± 0.029	0.986 ± 0.020

* C/E: calculated / experimental

Table 4.5 compares the multiplication factors obtained from TWODANT and MCNP4C calculations based on the ENDF/B-V.2 [40] and ENDF/B-VII.0 data. The MCNP4C Monte Carlo results show deviations from the benchmark experiment values by 200, 320, -60, 170, 370, and 630 pcm for the case A through F, respectively. For the cases A to D, the deviation is within one sigma uncertainty of the reference value, but for the cases E and F it is more than one sigma.

Table 4.5 Multiplication Factors for ZPPR-21 Phases A through F.

Benchmark Case		ENDF/B-V.2			ENDF/B-VII.0		
		VIM	TWODANT	Δk, pcm	MCNP4C	TWODANT	Δk, pcm
A	0.9967 ±0.0026	1.0000 ±0.0002	0.99873	-128	0.9987 ±0.0002	0.99864	-153
B	0.9897 ±0.0023	0.9925 ±0.0002	0.99293	43	0.9929 ±0.0002	0.99500	75
C	0.9998 ±0.0023	0.9979 ±0.0002	0.99698	-92	0.9992 ±0.0002	1.00008	-25
D	1.0018 ±0.0024	0.9997 ±0.0002	1.00042	72	1.0035 ±0.0002	1.00710	253
E	1.0012 ±0.0024	1.0000 ±0.0002	1.00008	8	1.0049 ±0.0002	1.00800	184
F	0.9998 ±0.0025	1.0005 ±0.0002	0.99852	-198	1.0061 ±0.0002	1.00717	11

The ZPPR-21 F core with all-uranium loading has the largest deviation among the six configurations. It is noted that ZPPR-21A was built with only plutonium fuel to take advantage of the inherent neutron source of Pu-240, and then enriched uranium was progressively substituted for plutonium in B through E, and finally F had all-uranium fuel loading. For both ENDF/B-V.2 and ENDF/B-VII.0 data, the MC^2-2/TWODANT results agree well with the MCNP4C Monte Carlo solutions. For ENDF/B-VII.0, the deviations from the MCNP4C results are -153, 75, -25, 253, 184, and 11 pcm for the case A through F, respectively. As shown in Figure 4.9, the trend of deviations in ENDF/B-VII.0 is similar to that in ENDF/B-V.2.

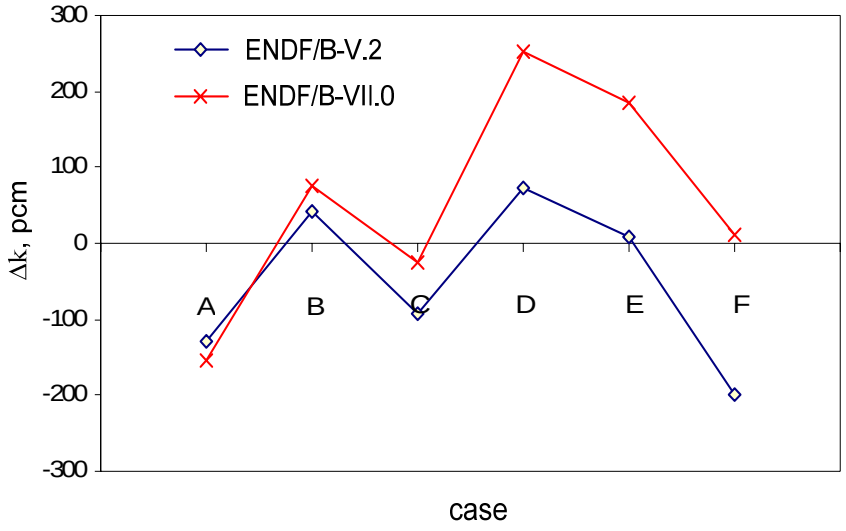

< pcm = [k_{eff}(reference) – k_{eff} (TWODANT)]*10^5 >
* Monte Carlo Code: VII for ENDF/B-V.2 and MCNP4C for ENDF/B-VII.0

Figure 4.9 Deviation of k-effective between Monte Carlo Codes and TWODANT for ZPPR-21 A through F.

In order to examine the potential reason why MC^2-2/TWODANT results show relatively large deviations from MCNP Monte Carlo solutions for the small-sized fast critical systems, the effect of anisotropy of elastic and inelastic scattering cross sections was investigated using the Godiva case. The VIM cross section libraries for the isotopes contained in Godiva were modified by making anisotropic elastic and inelastic scattering cross sections isotropic. As can be seen in Table 4.6, the effect of anisotropy of inelastic scattering cross sections is ~190 pcm which is

~75% of the original deviation with anisotropic scattering cross sections. This large anisotropy effect of inelastic scattering appears to be due to large leakage and very hard spectrum. This result suggests that the isotropic assumption of inelastic scattering in MC^2-2 needs to be improved in future.

Table 4.6 Multiplication Factors of Godiva with Change of Boundary and Scattering Conditions.

Condition	VIM	MC^2-2/TWODANT	%Δρ, pcm
Original condition	1.00095 ± 0.00070	1.00348	252
Reflective boundary condition	2.25854 ± 0.00034	2.26013	31
Isotropic elastic scattering	1.10084 ± 0.00071	1.10507	347
Isotropic elastic and inelastic scattering	1.10316 ± 0.00074	1.10507	157

5. Conclusion

Under the fast reactor simulation program launched in April 2007, development of an advanced multigroup cross section generation code was initiated in July 2007, in conjunction with the development of the high-fidelity deterministic neutron transport code UNIC. The general objectives are to simplify the existing multi-step schemes and to improve the resolved and unresolved resonance treatments.

Existing methods for multigroup cross section generation were reviewed in association with elastic slowing down treatment and resonance self-shielding calculation. Based on the review results and the fact that they have been applied successfully to fast critical experiment analyses and fast reactor designs for last three decades, the methodologies of the ETOE-2/MC^2-2/SDX code system were selected as the starting set of methodologies for multigroup cross section generation. For future extension to thermal reactor applications, the methodologies of the CENTRM/PMC system were also selected to be investigated.

In order to identify potential issues and improvement needs, the status of ETOE-2 and MC^2-2 codes was reviewed thoroughly, focused on enhancing accuracy and efficiency. Work initiated to implement the identified improvement needs, with this year's focus on the revision required to process the recently released ENDF/B-VII.0 data. Conversion in FORTRAN 90/95 was also initiated for eventual coupling with the UNIC code and use in a parallel computing environment. As the first step, the MC^2-2 code was updated by modernizing the memory structure and replacing old data management package subroutines and functions with FORTRAN 90 based routines. Various modifications were also made in the ETOE-2 and MC^2-2 codes to process the ENDF/B-VII.0 data properly, in relation to unresolved resonance data format, the multipole representation of resolved resonances, wide and weak resonance screening, fission neutron spectrum representation, shielding of resonance-like cross sections above the resonance energy region.

With the updated ETOE-2 code, the ENDF/B-VII.0 data was successfully processed for major heavy and intermediate nuclides employed in sodium-cooled fast reactors. Initial verification tests of the MC^2-2 libraries generated from ENDF/B-VII.0 data were performed by inter-comparison of twenty-one group infinite dilute total cross sections obtained from MC^2-2, VIM, and NJOY. The RABANL calculations were additionally carried out to obtain more

accurate representation of low-energy resolved resonance cross sections. Overall, the total cross sections of MC^2-2 agreed very well with those from VIM and/or NJOY. For some nuclides, however, differences up to 6% were noticed around the upper limit of the resolved resonance energy region. To identify the reason for this discrepancy, further investigation is being performed.

Preliminary validation tests of the ENDF/B-VII.0 libraries of MC^2-2 were also performed using a set of fast critical benchmark problems, including eight LANL fast critical assemblies, two ZPR fast critical assembles, and six ZPPR-21 critical assemblies. Using the 230-group multigroup cross section sets generated from MC^2-2 calculations, deterministic TWODANT calculations were performed. The TWODANT results agreed well with MCNP solutions within ~0.25% $\Delta\rho$, except a few small LANL fast critical assemblies. Relative to the MCNP solution, the TWODANT results overestimated the multiplication factor by 0.22 ~ 0.35% $\Delta\rho$ for these small systems with very hard neutron spectrum. Preliminary investigation indicated that a large portion of the underestimation of multiplication factor could be attributed to the isotropic assumption of inelastic scattering in the MC^2-2 methodologies. Comparisons of measured and calculated values for the fission reaction rate ratios of Godiva and Jezebel assemblies also showed that the TWODANT results agreed well with the measured values within 2.7%.

From a series of methodology review and ENDF/B- VII.0 data processing, several improvement needs to enhance accuracy were also identified for the ETOE-2/MC^2-2 code system, including the multigroup slowing solution for whole-energy range, proper treatment for anisotropy of inelastic scattering, improved evaluation of inelastic and high-order anisotropic scattering source in RABANL calculations.

References

1. G. Palmiotti, M. Smith, C. Rabiti, D. Kaushik, A. Siegel, B. Smith, and E. E. Lewis, "UNÌC: Ultimate Neutronic Investigation Code," *Proc. Intl Topical Meeting on Mathematics & Computation and Supercomputing in Nuclear Applications,* Monterey, California, April 15-19 (2007).
2. B. J. Toppel, H. Henryson II, and C. G. Stenberg, "ETOE-2/MC^2-2/SDX Multigroup Cross-Section Processing," Conf-780334-5, Presentation at RSIC Seminar Workshop on Multigroup Cross Sections, Oak Ridge, TN (March 1978).
3. H. Henryson II, B. J. Toppel, and C. G. Stenberg, "MC^2-2: A Code to Calculate Fast Neutron Spectra and Multigroup Cross Sections," ANL-8144, Argonne National Laboratory (1976).
4. M. L. Williams, M. Asgari, and D. F. Hollenbach, "CENTRM: A One-Dimensional Neutron Transport Code for Computing Pointwise Energy Spectra," ORNL/TM-2005/39, Vol. II, Book 4, Sect. F18 (April 2005).
5. M. L. Williams and D. F. Hollenbach, "PMC: A Program to Produce Multigroup Cross Section Using Pointwise Energy Spectra from CENTRM," ORNL/TM-2005/39, Vol. II, Book 4, Sect. F19 (April 2005).
6. P. Oblozinsky and M. Herman, "Special Issues on Evaluated Nuclear Data File ENDF/B-VII.0," *Nuclear Data Sheets*, **107**, 2931 (2006).
7. NEA Nuclear Science Committee, "International Handbook of Evaluated Criticality Safety Benchmark Experiments," NEA/NSC/DOC(95)03 (September 2006).
8. R. M. Lell, R. W. Schaefer, R. D. McKnight, and A. Mohamed, "ZPPR-21 Phase A: A Cylindrical Assembly of Pu Metal Reflected by Graphite," PU-MET-FAST-033, OECD/NEA, International Handbook of Evaluated Criticality Safety Benchmark Experiments, NEA/NSC/DOC(95)03 (2005).
9. R. D. McKnight, R. M. Lell, R. W. Schaefer, and A. Mohamed, "ZPPR-21 Phases B through E: Cylindrical Assemblies of Mixed Fissile Pu and U Metal Reflected by Graphite," MIX-MET-FAST-011, OECD/NEA, International Handbook of Evaluated Criticality Safety Benchmark Experiments, NEA/NSC/DOC(95)03 (2005).
10. R. W. Schaefer, R. D. McKnight, R. M. Lell, and A. Mohamed, "ZPPR-21 Phase F: A Cylindrical Assembly of U Metal Reflected by Graphite," HEU-MET-FAST-061, OECD/NEA, International Handbook of Evaluated Criticality Safety Benchmark Experiments, NEA/NSC/DOC(95)03 (2005).
11. I. I. Bondarenko, et al, *Group Constants for Nuclear Reactor Calculations*, Consultants Bureau Enterprises, Inc., New York (1964).
12. C. R. Weisbin et al, "MINX: A Multigroup Interpretation of Nuclear X-Sections from ENDF/B," LA-6486-MS, Los Alamos Scientific Laboratory (September 1976).
13. W. J. Davis, M. B. Yarbrough, and A. B. Bortz, "SPHINX, A One-Dimensional Diffusion and Transport Nuclear Cross Section Processing Code," WAPD-XS-3045-17, Westinghouse (1977).

14. MacFarlane, R. E., "NJOY 99/2001: New Capabilities in Data Processing," Presentation at the Workshop on Reactor Physics and Analysis Capabilities for Generation IV Nuclear Energy Systems, Argonne National Laboratory, Argonne, Illinois, February 18-19, (2003).
15. A. E. Waltar and A. B. Reynolds, *Fast Breeder Reactor*, Pergamon Press (1981).
16. Y. Ronen, et al, *CRC Handbook of Nuclear Reactors Calculations*, CRC Press, Inc. (1987).
17. H. H. Hummel and D. Okrent, *Reactivity Coefficients in Large Fast Power Reactors*, Monograph series on nuclear science and technology, American Nuclear Society (1970).
18. R. N. Hwang, *Nucl. Sci. Eng.* **52,** 157 (1973).
19. G. Goertzel and E. Greuling, *Nucl. Sci. Eng.* **7**, 69 (1960).
20. W. M. Stacey, Jr., "Advances in Continuous Slowing-Down Theory," *Proc. Natl Topical Meeting on New Developments in Reactor Physics and Shielding*, Conf-720901 Book 1, 143 (1972).
21. H. H. Hummel, R. N. Hwang and K. Phillips, "Recent Investigations of Fast Reactor Reactivity Coefficients", *Proc. Conf. On Safety, Fuels, and Core Design in Large Fast Power Reactors*, p. 413-420, ANL-7120 (1965).
22. A. Hebert, "A Review of Legacy and Advanced Self-Shielding Models for Lattice Calculations," *Nucl. Sci. Eng.*, **155**, 310 (2007).
23. L. B. Levitt, "The Probability Table Method for Treating Unresolved Resonances in Monte Carlo Criticality Calculations," *Trans. Am. Nucl. Soc.* **14**, 648 (1971).
24. M. N. Nikolaev, et al. *Atomn. Energ.* **29**, 11 (1970); ibcd, *Atomn. Energ.* **30**, 426 (1971).
25. D. E. Cullen, *Nucl. Sci. Eng.* **55**, 378 (1974).
26. P. Ribon and J. M. Maillard, *Les Tables De Probabilite Applications Au Traitement Des Sections Efficaces Pour La Neutronique*, Report CEA-N, NEACRP-L-294 (1986).
27. M. D. DeHart, "NEWT: A New Transport Algorithm for Two-Dimensional Discrete Ordinates Geometries," ORNL/TM-2005/39, Vol. II, Book 4, Sect. F21 (April 2005)
28. Z. Zhaopeng, et al, "Continuous-Energy Multidimensional S_N Transport for Problem-Dependent Resonance Self-Shielding Calculations," *Nucl. Sci. Eng.* **154**, 190 (2006).
29. R. N. Hwang, "A Rigorous Pole Representation of Multilevel Cross Sections and Its Practical Applications," *Nucl. Sci. Eng.*, **96**, 192 (1987).
30. R. N. Hwang, "An Extension of the Rigorous Pole Representation of Cross Sections for Reactor Applications," *Nucl. Sci. Eng.*, **111**, 113 (1992).
31. F. J. Dyson, *J. Math. Phys.* **3**, No. 1, 140 (1962).
32. C. Stenberg, R. McKnight, "Verification and Validation of Fast Systems with ENDF/B Data," ANS Nuclear Criticality Safety Division Embedded Topical Meeting, Reno, Nevada, Nov. 11-15 (2001).
33. L. C. Just, el al., "The System Aspects and Interface Data Sets of the Argonne Reactor Computation (ARC) System," ANL-7711 (1971).
34. R. N. Hwang, Private Communication, Argonne National Laboratory (August 2002).

35. Cross Section Evaluation Working Group, "ENDF-6 Formats Manual: Data Formats and Procedures for the Evaluated Nuclear Data File ENDF/B-VI and ENDF/B-VII," National Nuclear Data Center, Brookhaven National Laboratory, BNL-NCS-44945-05-Rev, June (2005).
36. R. N. Hwang, B. J. Toppel, and H. Henryson II, "Improved Algorithms for the Calculation of Resolved Resonance Cross Sections with Application to the Structural Doppler Effect," ANL-80-104, Argonne National Laboratory (October 1980).
37. R. N. Blomquist, "VIM Continuous Energy Monte Carlo Transport Code," *Proc. Intl. Conf. on Mathematics, Computations, Reactor Physics and Environmental Analysis,* Portland, OR, April 30-May 4 (1995).
38. Alcouffe, R. E., Brinkley, F. W., Marr, D. R., and O'Dell, R. D., "User's Guide for TWODANT: A Code Package for Two-Dimensional, Diffusion-Accelerated, Neutral-Particle Transport," LA-10049-M, Los Alamos National Laboratory (1990).
39. "MCNP – A General Monte Carlo N-Particle Transport Code," Version 5, LA-UR-03-1987, Los Alamos National Laboratory (April 2003).
40. W. S. Yang, et al, Private Communication, Argonne National Laboratory, (April 2007).

Appendix A. Resonance Data and Total Cross Sections of Nuclides in ENDF/B-VII.0

Table A.1 Resonance Data of Major Nuclides in ENDF/B-VII.0.

Isotope	Resolved				Unresolved	Isotope	Resolved				Unresolved
	Type*	Original Number	Remaining after Screened	Upper Energy Boundary (keV)	Upper Energy Boundary (keV)		Type*	Original Number	Remaining after Screened	Upper Energy Boundary (keV)	Upper Energy Boundary (keV)
Na-23	MB	23	9	500	-	Mo-96	MB	75	62	19	100
Cr-50	RM	386	321	792	-	Mo-97	MB	66	55	2	100
Cr-52	RM	223	173	980	-	Mo-98	MB	158	109	32	100
Cr-53	RM	131	113	200	-	Mo-100	MB	124	99	26	100
Cr-54	RM	116	99	900	-	Th-232	RM	927	464	4	100
Fe-54	RM	380	351	700	-	U-233	RM	770	546	0.6	40
Fe-56	RM	311	279	850	-	U-234	MB	119	118	1.5	100
Fe-57	RM	75	82	200	-	U-235	RM	3193	2409	2.25	25
Fe-58	RM	68	84	400	-	U-236	RM	117	116	1.5	100
Mn-55	MB	149	89	100	-	U-238	RM	3343	2216	20	149
Ni-58	RM	482	415	812	-	Np-237	MB	760	545	0.5	35
Ni-60	RM	272	254	450	-	Pu-238	SB	16	14	0.2	10
Ni-61	RM	32	19	70	-	Pu-239	RM	1070	691	2.5	30
Ni-62	RM	57	37	600	-	Pu-240	MB	268	263	5.7	40
Ni-64	RM	52	30	600	-	Pu-241	RM	244	216	0.3	40.2
Ga-69	MB	27	15	4.5	-	Pu-242	SB	68	67	1.0	10
Ga-71	MB	30	16	5.6	-	Am-241	SB	195	186	0.2	30
Zr-90	MB	89	17	60	400	Am-242m	MB	106	98	0.04	27.3
Zr-91	MB	95	80	20	100	Am-243	SB	220	216	0.3	42.4
Zr-92	MB	101	60	71	100	Cm-242	SB	12	12	0.3	10
Zr-94	MB	73	52	90	100	Cm-243	SB	105	99	0.1	42.2
Zr-96	MB	30	13	100	-	Cm-244	MB	68	67	1	40
Mo-92	MB	77	64	50	100	Cm-245	MB	91	78	0.1	55
Mo-94	MB	55	46	20	100	Cm-246	MB	17	17	0.4	43
Mo-95	MB	56	46	2.1	206.3	-	-	-	-	-	-

* SB: Single-level Breit-Wigner, MB: Multi-level Breit-Wigner, AA: Adler-Adler, RM: Reich-Moore.

Table A.2 Comparison of Total Cross Sections for U-233 and U-234.

		U-233				U-234			
Group	Energy(eV)	VIM(barn)	VIM vs MC2-2(%diff)	VIM vs MC2-2R(%diff)	NJOY vs MC2-2(%diff)	VIM(barn)	VIM vs MC2-2(%diff)	VIM vs MC2-2R(%diff)	NJOY vs MC2-2(%diff)
1	1.414E+07	6.638E+00	-0.27	-0.27		6.572E+00	-0.27	-0.27	
2	6.065E+06	7.745E+00	-0.01	-0.01	0.17	7.665E+00	-0.01	-0.01	0.16
3	3.679E+06	7.571E+00	0.04	0.04		7.596E+00	0.03	0.03	
4	2.231E+06	6.992E+00	0.02	0.02	0.14	7.052E+00	0.02	0.02	0.13
5	1.353E+06	6.791E+00	0.00	0.00	0.02	6.896E+00	-0.01	-0.01	-0.03
6	8.209E+05	7.657E+00	0.00	0.00	0.03	7.801E+00	0.00	0	0.03
7	4.979E+05	9.040E+00	-0.01	-0.01	0.08	9.148E+00	-0.01	-0.01	0.10
8	3.020E+05	1.053E+01	0.02	0.02	0.18	1.063E+01	0.02	0.02	0.17
9	1.490E+05	1.152E+01	0.02	0.02	0.02	1.157E+01	0.01	0.01	0.02
10	1.111E+05	1.219E+01	0.00	0.00	0.00	1.023E+01	**10.48**	**10.48**	**-0.04**
11	6.738E+04	1.304E+01	0.00	0.00	0.00	1.151E+01	-0.60	-0.6	-0.05
12	4.087E+04	1.405E+01	0.00	0.00	0.00	1.204E+01	-0.51	-0.51	-0.04
13	2.500E+04	1.480E+01	0.01	0.00	0.00	1.295E+01	-0.30	-0.31	-0.04
14	1.503E+04	1.556E+01	0.02	0.02	0.00	1.401E+01	-0.01	-0.01	-0.03
15	1.000E+04	1.665E+01	-0.01	-0.01	0.00	1.523E+01	-0.17	-0.17	-0.02
16	5.531E+03	1.805E+01	0.02	0.02	0.00	1.678E+01	-0.29	-0.29	-0.02
17	3.355E+03	1.951E+01	-0.03	-0.04	-0.03	1.879E+01	-0.39	-0.4	-0.05
18	2.500E+03	2.170E+01	-0.05	-0.05	-0.02	2.028E+01	-1.88	-0.26	-1.65
19	1.234E+03	2.649E+01	-1.15	0.23	-1.14	2.337E+01	-0.01	-0.35	0.34
20	4.540E+02	4.268E+01	-2.41	1.06	-2.43	4.222E+01	1.10	-0.23	1.34
21	6.144E+01	1.792E+02	13.92	0.30	13.90	1.449E+02	25.78	-3.89	25.43

* Yellow color denotes the unresolved resonance region, gray color denotes the resolved resonance region, and MC^2-2R represents the MC^2-2 calculation with RABANL option.

Table A.3 Comparison of Total Cross Sections for U-235 and U-236.

		U-235				U-236			
Group	Energy(eV)	VIM(barn)	VIM vs MC2-2(%diff)	VIM vs MC2-2R(%diff)	NJOY vs MC2-2(%diff)	VIM(barn)	VIM vs MC2-2(%diff)	VIM vs MC2-2R(%diff)	NJOY vs MC2-2(%diff)
1	1.414E+07	6.638E+00	-0.26	-0.26		6.611E+00	-0.27	-0.27	
2	6.065E+06	7.743E+00	-0.01	-0.01	0.17	7.721E+00	-0.01	-0.01	0.16
3	3.679E+06	7.556E+00	0.04	0.04		7.679E+00	0.03	0.03	
4	2.231E+06	6.962E+00	0.02	0.02	0.14	7.139E+00	0.02	0.02	0.13
5	1.353E+06	6.787E+00	-0.01	-0.01	-0.05	6.947E+00	-0.01	-0.01	-0.02
6	8.209E+05	7.631E+00	0.00	0.00	0.03	7.854E+00	0.00	0.00	0.03
7	4.979E+05	8.867E+00	-0.01	-0.01	0.14	9.217E+00	-0.01	-0.01	0.10
8	3.020E+05	1.044E+01	0.01	0.01	0.19	1.125E+01	0.02	0.02	0.28
9	1.490E+05	1.149E+01	0.02	0.02	0.02	1.310E+01	0.03	0.03	0.03
10	1.111E+05	1.222E+01	0.00	0.00	0.00	1.380E+01	-0.50	-0.50	-0.07
11	6.738E+04	1.308E+01	0.00	0.00	0.00	1.400E+01	-0.67	-0.67	-0.08
12	4.087E+04	1.384E+01	0.00	0.00	0.00	1.442E+01	-0.63	-0.63	-0.08
13	2.500E+04	1.470E+01	0.01	0.04	0.00	1.509E+01	-0.70	-0.70	-0.08
14	1.503E+04	1.553E+01	0.00	0.00	0.00	1.583E+01	-0.64	-0.64	-0.09
15	1.000E+04	1.652E+01	0.00	0.00	0.00	1.690E+01	-0.62	-0.62	-0.06
16	5.531E+03	1.769E+01	0.00	0.00	0.00	1.842E+01	-0.49	-0.49	-0.06
17	3.355E+03	1.853E+01	-0.02	-0.03	-0.05	1.989E+01	-0.69	-0.69	-0.11
18	2.500E+03	2.125E+01	**-3.89**	**-9.88**	**-3.92**	2.200E+01	-1.62	-0.34	-1.39
19	1.234E+03	2.750E+01	0.50	-0.66	0.50	2.790E+01	-0.08	-0.04	-0.02
20	4.540E+02	4.159E+01	0.19	1.00	0.16	4.773E+01	1.68	-0.14	1.83
21	6.144E+01	7.884E+01	2.72	-0.08	2.75	7.909E+01	29.39	2.60	29.05

* Yellow color denotes the unresolved resonance region, gray color denotes the resolved resonance region, and MC^2-2R represents the MC^2-2 calculation with RABANL option.

Table A.4 Comparison of Total Cross Sections for U-238 and Np-237.

		U-238				Np-237			
Group	Energy(eV)	VIM(barn)	VIM vs MC2-2(%diff)	VIM vs MC2-2R(%diff)	NJOY vs MC2-2(%diff)	VIM(barn)	VIM vs MC2-2(%diff)	VIM vs MC2-2R(%diff)	NJOY vs MC2-2(%diff)
1	1.414E+07	6.702E+00	-0.26	-0.26		6.559E+00	-0.25	-0.25	
2	6.065E+06	7.773E+00	-0.01	-0.01	0.16	7.619E+00	-0.01	-0.01	0.15
3	3.679E+06	7.633E+00	0.03	0.03		7.416E+00	0.03	0.03	
4	2.231E+06	7.133E+00	0.01	0.01	0.12	6.940E+00	0.01	0.01	0.11
5	1.353E+06	7.050E+00	-0.01	-0.01	-0.06	6.784E+00	-0.01	-0.01	-0.03
6	8.209E+05	7.888E+00	0.00	0.00	0.02	7.602E+00	0.00	0.00	0.02
7	4.979E+05	9.091E+00	-0.01	-0.01	0.11	8.826E+00	-0.01	-0.01	0.11
8	3.020E+05	1.050E+01	0.02	0.02	0.17	1.025E+01	0.02	0.02	0.18
9	1.490E+05	1.163E+01	0.00	0.00	0.02	1.125E+01	0.01	0.01	0.02
10	1.111E+05	1.229E+01	0.00	0.00	0.00	1.190E+01	**1.86**	**1.86**	**0.00**
11	6.738E+04	1.300E+01	0.00	0.00	0.00	1.267E+01	**4.53**	**4.53**	**0.00**
12	4.087E+04	1.364E+01	0.03	0.03	0.00	1.346E+01	**5.21**	**5.21**	**-0.03**
13	2.500E+04	1.455E+01	**-6.22**	**-4.71**	**-6.34**	1.428E+01	**5.92**	**5.92**	**-0.03**
14	1.503E+04	1.518E+01	**-2.68**	**-5.53**	**-2.69**	1.510E+01	**6.46**	**6.46**	**-0.02**
15	1.000E+04	1.591E+01	-0.12	-0.30	-0.14	1.638E+01	**5.27**	**5.27**	**-0.01**
16	5.531E+03	1.789E+01	-0.51	0.05	-0.55	1.780E+01	**5.83**	**5.83**	**-0.01**
17	3.355E+03	2.246E+01	1.14	0.38	1.17	1.914E+01	**5.83**	**5.83**	**-0.03**
18	2.500E+03	2.314E+01	5.16	-0.20	5.19	2.132E+01	**5.65**	**5.65**	**-0.03**
19	1.234E+03	2.345E+01	9.83	0.26	9.56	2.656E+01	**4.08**	**4.71**	**-0.61**
20	4.540E+02	5.734E+01	3.35	0.49	2.84	4.569E+01	**4.45**	**4.82**	**-0.35**
21	6.144E+01	7.608E+01	3.97	0.35	3.60	1.643E+02	**4.68**	**1.08**	**3.51**

* Yellow color denotes the unresolved resonance region, gray color denotes the resolved resonance region, and MC^2-2R represents the MC^2-2 calculation with RABANL option.

Table A.5 Comparison of Total Cross Sections for Pu-238 and Pu-239.

		Pu-238				Pu-239			
Group	Energy(eV)	VIM(barn)	VIM vs MC2-2(%diff)	VIM vs MC2-2R(%diff)	NJOY vs MC2-2(%diff)	VIM(barn)	VIM vs MC2-2(%diff)	VIM vs MC2-2R(%diff)	NJOY vs MC2-2(%diff)
1	1.414E+07	6.702E+00	-0.01	-0.01		6.638E+00	-0.24	-0.24	
2	6.065E+06	7.773E+00	-0.02	-0.02	-0.01	7.743E+00	-0.01	-0.01	0.17
3	3.679E+06	7.633E+00	0.03	0.03		7.556E+00	0.03	0.03	
4	2.231E+06	7.133E+00	0.02	0.02	0.10	6.962E+00	0.01	0.01	0.12
5	1.353E+06	7.050E+00	0.00	0.00	-0.10	6.787E+00	-0.01	-0.01	-0.01
6	8.209E+05	7.888E+00	0.00	0.00	0.03	7.631E+00	0.00	0.00	0.03
7	4.979E+05	9.091E+00	-0.01	-0.01	0.21	8.867E+00	-0.01	-0.01	0.12
8	3.020E+05	1.050E+01	0.02	0.02	0.24	1.044E+01	0.01	0.01	0.17
9	1.490E+05	1.163E+01	0.02	0.02	0.02	1.149E+01	0.02	0.02	0.02
10	1.111E+05	1.229E+01	0.00	0.00	0.00	1.222E+01	0.00	0.00	0.00
11	6.738E+04	1.300E+01	0.00	0.00	0.00	1.308E+01	0.00	0.00	0.00
12	4.087E+04	1.364E+01	0.01	0.00	0.00	1.384E+01	**2.53**	**2.53**	**-0.71**
13	2.500E+04	1.455E+01	0.00	0.00	0.00	1.470E+01	-0.61	-0.62	-0.02
14	1.503E+04	1.518E+01	0.01	0.01	0.01	1.553E+01	-0.55	-0.55	-0.01
15	1.000E+04	1.591E+01	**-6.70**	**-6.70**	**-0.27**	1.652E+01	-0.53	-0.53	-0.01
16	5.531E+03	1.789E+01	**-12.99**	**-12.99**	**-0.44**	1.769E+01	-1.38	-1.38	-0.01
17	3.355E+03	2.246E+01	**-14.60**	**-14.60**	**-0.54**	1.853E+01	-0.51	-0.51	-0.01
18	2.500E+03	2.314E+01	**-13.80**	**-13.80**	**-0.55**	2.125E+01	**-2.21**	**-1.82**	**-2.21**
19	1.234E+03	2.345E+01	**-6.27**	**-6.28**	**-0.49**	2.750E+01	**0.54**	**-2.68**	**0.60**
20	4.540E+02	5.734E+01	-0.39	-0.57	-1.57	4.159E+01	1.00	-3.93	1.04
21	6.144E+01	7.608E+01	8.56	-0.28	8.72	7.884E+01	**5.62**	**-2.62**	**5.61**

* Yellow color denotes the unresolved resonance region, gray color denotes the resolved resonance region, and MC^2-2R represents the MC^2-2 calculation with RABANL option.

Table A.6 Comparison of Total Cross Sections for Pu-240 and Pu-241.

		Pu-240				Pu-241			
Group	Energy(eV)	VIM(barn)	VIM vs MC2-2(%diff)	VIM vs MC2-2R(%diff)	NJOY vs MC2-2(%diff)	VIM(barn)	VIM vs MC2-2(%diff)	VIM vs MC2-2R(%diff)	NJOY vs MC2-2(%diff)
1	1.414E+07	6.640E+00	-0.25	-0.25		6.682E+00	-0.24	-0.24	
2	6.065E+06	7.717E+00	-0.01	-0.01	0.17	7.789E+00	-0.01	-0.01	0.14
3	3.679E+06	7.676E+00	0.03	0.03		7.640E+00	0.03	0.03	
4	2.231E+06	7.200E+00	0.01	0.01	0.11	7.153E+00	0.01	0.01	0.10
5	1.353E+06	7.066E+00	-0.01	-0.01	-0.04	7.003E+00	-0.01	-0.01	-0.06
6	8.209E+05	7.989E+00	0.00	0.00	0.03	7.808E+00	0.00	0.00	0.02
7	4.979E+05	9.335E+00	-0.01	-0.01	0.07	8.873E+00	-0.01	-0.01	0.08
8	3.020E+05	1.068E+01	0.01	0.01	0.14	1.008E+01	0.02	0.02	0.15
9	1.490E+05	1.151E+01	0.01	0.01	0.01	1.101E+01	0.02	0.02	0.02
10	1.111E+05	1.206E+01	0.00	0.00	0.00	1.181E+01	0.00	0.00	0.00
11	6.738E+04	1.220E+01	**3.85**	**3.85**	**0.00**	1.285E+01	0.00	0.00	0.00
12	4.087E+04	1.286E+01	**3.17**	**3.17**	**-0.05**	1.397E+01	-0.88	-0.89	-0.04
13	2.500E+04	1.411E+01	-0.62	-0.62	-0.04	1.487E+01	-0.51	-0.51	-0.04
14	1.503E+04	1.495E+01	-0.52	-0.52	-0.03	1.567E+01	-0.47	-0.48	-0.03
15	1.000E+04	1.640E+01	-1.47	-0.52	-0.98	1.682E+01	-0.46	-0.46	-0.02
16	5.531E+03	1.570E+01	-2.06	-0.02	-2.04	1.878E+01	-0.21	-0.21	-0.01
17	3.355E+03	1.690E+01	-2.78	0.25	-2.67	2.030E+01	-0.32	-0.32	-0.03
18	2.500E+03	1.989E+01	1.01	-0.17	1.00	2.283E+01	-0.24	-0.24	-0.04
19	1.234E+03	2.207E+01	4.79	-0.04	4.84	2.766E+01	-0.23	-0.24	0.00
20	4.540E+02	7.141E+01	0.52	0.15	0.38	5.091E+01	-2.58	1.43	-2.57
21	6.144E+01	1.839E+03	31.36	2.78	31.25	1.434E+02	-0.93	0.54	-0.93

* Yellow color denotes the unresolved resonance region, gray color denotes the resolved resonance region, and MC^2-2R represents the MC^2-2 calculation with RABANL option.

Table A.7 Comparison of Total Cross Sections for Pu-242 and Am-241.

		Pu-242				Am-241			
Group	Energy(eV)	VIM(barn)	VIM vs MC2-2(%diff)	VIM vs MC2-2R(%diff)	NJOY vs MC2-2(%diff)	VIM(barn)	VIM vs MC2-2(%diff)	VIM vs MC2-2R(%diff)	NJOY vs MC2-2(%diff)
1	1.414E+07	6.867E+00	-0.29	-0.29		6.780E+00	-0.27	-0.27	
2	6.065E+06	7.850E+00	-0.01	-0.01	0.15	7.643E+00	-0.01	-0.01	0.14
3	3.679E+06	7.546E+00	0.03	0.03		7.332E+00	0.03	0.03	
4	2.231E+06	7.140E+00	0.01	0.01	0.09	6.866E+00	0.01	0.01	0.12
5	1.353E+06	7.270E+00	-0.01	-0.01	-0.10	7.001E+00	-0.02	-0.02	-0.10
6	8.209E+05	8.374E+00	0.00	0.00	0.03	8.073E+00	0.00	0.00	0.02
7	4.979E+05	9.833E+00	-0.01	-0.01	0.08	9.559E+00	-0.01	-0.01	0.08
8	3.020E+05	1.134E+01	0.01	0.01	0.16	1.103E+01	0.01	0.01	0.15
9	1.490E+05	1.225E+01	0.01	0.01	0.01	1.194E+01	0.01	0.01	0.01
10	1.111E+05	1.277E+01	0.00	0.00	0.00	1.256E+01	0.00	0.00	0.00
11	6.738E+04	1.329E+01	-0.01	-0.01	0.00	1.331E+01	0.00	0.00	0.00
12	4.087E+04	1.377E+01	0.00	0.00	0.00	1.416E+01	-0.42	-0.42	-0.02
13	2.500E+04	1.432E+01	0.00	-0.01	0.00	1.486E+01	-0.88	-0.88	-0.04
14	1.503E+04	1.496E+01	0.00	-0.01	0.00	1.529E+01	-0.70	-0.70	-0.03
15	1.000E+04	1.524E+01	-0.66	-0.66	-0.20	1.613E+01	-0.61	-0.62	-0.02
16	5.531E+03	1.647E+01	-1.02	-1.02	-1.43	1.750E+01	-0.45	-0.45	-0.02
17	3.355E+03	1.748E+01	-1.09	-1.10	-2.35	1.939E+01	-0.36	-0.37	-0.03
18	2.500E+03	1.916E+01	-1.02	-1.02	-1.42	2.173E+01	-0.43	-0.43	-0.04
19	1.234E+03	2.556E+01	-1.68	-0.02	-1.84	2.581E+01	-0.21	-0.21	0.00
20	4.540E+02	2.895E+01	0.80	0.05	0.75	4.498E+01	-0.83	0.05	-0.89
21	6.144E+01	2.948E+02	27.48	1.06	27.35	2.853E+02	9.83	-0.23	9.87

* Yellow color denotes the unresolved resonance region, gray color denotes the resolved resonance region, and MC^2-2R represents the MC^2-2 calculation with RABANL option.

Table A.8 Comparison of Total Cross Sections for Am-242m and Am-243.

		Am-242				Am243			
Group	Energy(eV)	VIM(barn)	VIM vs MC2-2(%diff)	VIM vs MC2-2R(%diff)	NJOY vs MC2-2(%diff)	VIM(barn)	VIM vs MC2-2(%diff)	VIM vs MC2-2R(%diff)	NJOY vs MC2-2(%diff)
1	1.414E+07	6.702E+00				6.537E+00	-0.25	-0.25	
2	6.065E+06	7.773E+00			0.13	7.537E+00	-0.01	-0.01	0.15
3	3.679E+06	7.633E+00				7.479E+00	0.03	0.03	
4	2.231E+06	7.133E+00			0.12	7.066E+00	0.01	0.01	0.10
5	1.353E+06	7.050E+00			-0.05	7.103E+00	-0.01	-0.01	-0.09
6	8.209E+05	7.888E+00			0.02	8.076E+00	0.00	0.00	0.03
7	4.979E+05	9.091E+00			0.11	9.418E+00	-0.01	-0.01	0.12
8	3.020E+05	1.050E+01			0.18	1.099E+01	0.02	0.02	0.18
9	1.490E+05	1.163E+01			0.02	1.203E+01	0.01	0.01	0.01
10	1.111E+05	1.229E+01	Not Available		0.00	1.264E+01	0.00	0.00	0.00
11	6.738E+04	1.300E+01			0.00	1.343E+01	-0.18	-0.18	-0.01
12	4.087E+04	1.364E+01			-0.02	1.474E+01	-1.72	-1.72	-0.13
13	2.500E+04	1.455E+01			-0.09	1.533E+01	-1.17	-1.17	-0.13
14	1.503E+04	1.518E+01			-0.07	1.602E+01	-0.89	-0.89	-0.21
15	1.000E+04	1.591E+01			-0.14	1.700E+01	-0.71	-0.71	-0.13
16	5.531E+03	1.789E+01			-0.10	1.842E+01	-0.67	-0.67	-0.29
17	3.355E+03	2.246E+01			-0.12	1.972E+01	-0.63	-0.64	-0.33
18	2.500E+03	2.314E+01			-0.15	2.185E+01	-0.60	-0.61	-0.39
19	1.234E+03	2.345E+01			-0.14	2.704E+01	-0.53	-0.53	-0.42
20	4.540E+02	5.734E+01			-0.28	4.395E+01	-1.09	-0.14	-1.01
21	6.144E+01	7.608E+01			23.60	3.673E+02	22.59	-0.28	22.74

* Yellow color denotes the unresolved resonance region, gray color denotes the resolved resonance region, and MC^2-2R represents the MC^2-2 calculation with RABANL option.

Table A.9 Comparison of Total Cross Sections for Th-232 and Na-23.

		Th-232				Na-23			
Group	Energy(eV)	VIM(barn)	VIM vs MC2-2(%diff)	VIM vs MC2-2R(%diff)	NJOY vs MC2-2(%diff)	VIM(barn)	VIM vs MC2-2(%diff)	VIM vs MC2-2R(%diff)	NJOY vs MC2-2(%diff)
1	1.414E+07	5.995E+00				1.789E+00	-0.01	-0.01	
2	6.065E+06	7.684E+00			0.18	2.068E+00	0.03	0.03	-0.32
3	3.679E+06	7.604E+00				2.746E+00	-0.01	-0.01	
4	2.231E+06	7.056E+00			0.13	2.817E+00	0.19	0.19	1.50
5	1.353E+06	6.926E+00			-0.03	3.747E+00	0.07	0.07	-0.77
6	8.209E+05	7.803E+00			0.03	5.005E+00	0.12	0.12	0.04
7	4.979E+05	9.187E+00			0.13	3.444E+00	-0.90	-0.90	-3.75
8	3.020E+05	1.083E+01			0.19	3.988E+00	-0.96	-0.96	-0.07
9	1.490E+05	1.195E+01			0.02	3.414E+00	-0.25	-0.25	-0.19
10	1.111E+05	1.267E+01			0.00	3.623E+00	0.01	0.01	0.11
11	6.738E+04	1.344E+01	Not Available		0.00	5.877E+00	-1.36	-1.36	0.20
12	4.087E+04	1.411E+01			0.00	4.073E+00	-0.07	-0.07	-0.03
13	2.500E+04	1.480E+01			0.00	4.280E+00	0.05	0.05	0.05
14	1.503E+04	1.552E+01			0.00	4.775E+00	0.05	0.05	0.05
15	1.000E+04	1.643E+01			0.00	6.235E+00	0.05	0.05	0.02
16	5.531E+03	1.624E+01			-2.88	1.896E+01	-0.02	-0.02	0.02
17	3.355E+03	1.949E+01			-4.87	1.978E+02	0.42	0.42	0.46
18	2.500E+03	2.147E+01			0.52	1.559E+01	1.61	1.61	1.55
19	1.234E+03	2.371E+01			2.80	3.517E+00	-0.27	-0.27	-0.03
20	4.540E+02	4.956E+01			1.80	3.175E+00	0.00	0.00	-0.01
21	6.144E+01	2.340E+01			5.25	3.214E+00	0.00	0.00	-0.03

* Yellow color denotes the unresolved resonance region, gray color denotes the resolved resonance region, and MC^2-2R represents the MC^2-2 calculation with RABANL option.

Table A.10 Comparison of Total Cross Sections for Cm-242 and Cm-244.

		Cm-242				Cm-244			
Group	Energy(eV)	VIM(barn)	VIM vs MC2-2(%diff)	VIM vs MC2-2R(%diff)	NJOY vs MC2-2(%diff)	VIM(barn)	VIM vs MC2-2(%diff)	VIM vs MC2-2R(%diff)	NJOY vs MC2-2(%diff)
1	1.414E+07	6.541E+00	-0.14	-0.14		6.798E+00	-0.28	-0.28	
2	6.065E+06	7.157E+00	-0.01	-0.01	0.14	7.695E+00	-0.02	-0.02	0.15
3	3.679E+06	7.417E+00	0.00	0.00		7.358E+00	0.02	0.02	
4	2.231E+06	6.932E+00	0.03	0.03	0.16	6.973E+00	0.01	0.01	0.08
5	1.353E+06	6.542E+00	0.00	0.00	-0.35	7.044E+00	-0.03	-0.03	-0.04
6	8.209E+05	7.162E+00	0.00	0.00	0.02	8.167E+00	-0.04	-0.04	0.02
7	4.979E+05	9.141E+00	-0.01	-0.01	0.21	9.843E+00	-0.07	-0.07	0.15
8	3.020E+05	1.086E+01	0.01	0.01	0.15	1.155E+01	0.00	0.00	0.15
9	1.490E+05	1.201E+01	0.03	0.03	0.03	1.239E+01	0.00	0.00	0.01
10	1.111E+05	1.261E+01	0.00	0.00	0.00	1.277E+01	-0.01	-0.01	0.00
11	6.738E+04	1.278E+01	0.00	0.00	0.00	1.309E+01	0.00	0.00	0.00
12	4.087E+04	1.274E+01	0.00	0.00	0.00	1.351E+01	-0.63	-0.63	-0.10
13	2.500E+04	1.279E+01	0.00	0.00	0.00	1.395E+01	-0.65	-0.65	-0.29
14	1.503E+04	1.290E+01	0.02	0.02	0.01	1.450E+01	-0.64	-0.64	-0.43
15	1.000E+04	1.462E+01	-0.59	-0.59	-0.20	1.529E+01	-0.63	-0.64	-0.20
16	5.531E+03	1.588E+01	-0.97	-0.97	-1.44	1.650E+01	-0.59	-0.59	-0.15
17	3.355E+03	1.704E+01	-1.27	-1.27	-2.35	1.761E+01	-0.36	-0.37	-0.33
18	2.500E+03	1.874E+01	-0.76	-0.76	-1.38	1.962E+01	-0.80	-0.80	-1.26
19	1.234E+03	2.308E+01	-0.55	-0.55	-0.51	3.628E+01	-2.07	0.09	-2.27
20	4.540E+02	2.925E+01	-1.47	-0.23	-1.61	4.005E+01	4.34	0.19	4.15
21	6.144E+01	2.921E+01	1.74	-0.06	1.80	1.686E+02	31.33	-0.59	31.12

* Yellow color denotes the unresolved resonance region, gray color denotes the resolved resonance region, and MC^2-2R represents the MC^2-2 calculation with RABANL option.

Table A.11 Comparison of Total Cross Sections for Cr-50 and Cr-52.

		Cr-50				Cr-52			
Group	Energy(eV)	VIM(barn)	VIM vs MC2-2(%diff)	VIM vs MC2-2R(%diff)	NJOY vs MC2-2(%diff)	VIM(barn)	VIM vs MC2-2(%diff)	VIM vs MC2-2R(%diff)	NJOY vs MC2-2(%diff)
1	1.414E+07	3.396E+00	-0.29	-0.29		3.397E+00	-0.28	-0.28	
2	6.065E+06	3.671E+00	0.02	0.02	0.29	3.701E+00	0.01	0.01	0.29
3	3.679E+06	3.716E+00	-0.11	-0.11		3.492E+00	0.27	0.27	
4	2.231E+06	3.293E+00	-0.03	-0.03	0.21	3.282E+00	-0.01	-0.01	0.45
5	1.353E+06	3.318E+00	0.18	0.51	1.74	3.108E+00	-0.38	0.15	-0.58
6	8.209E+05	3.642E+00	-0.22	-0.12	-0.25	3.105E+00	-0.96	0.03	-1.04
7	4.979E+05	4.204E+00	0.72	-3.59	0.40	3.622E+00	0.04	-7.66	0.88
8	3.020E+05	3.741E+00	-0.18	-0.52	0.04	4.212E+00	0.63	-0.99	1.74
9	1.490E+05	4.008E+00	-1.84	0.27	-1.80	6.402E+00	-0.33	-0.09	-0.38
10	1.111E+05	5.136E+00	0.43	0.24	0.40	6.058E+00	0.08	0.59	0.03
11	6.738E+04	8.489E+00	2.21	1.65	2.21	7.130E+00	0.00	0.16	0.01
12	4.087E+04	1.524E+01	2.72	2.54	2.69	2.276E+00	-0.39	-0.05	-0.37
13	2.500E+04	4.440E+00	0.74	-0.11	0.79	2.820E+00	0.40	0.03	0.39
14	1.503E+04	1.424E+01	0.32	0.06	0.29	2.637E+00	0.01	0.01	0.01
15	1.000E+04	1.552E+02	0.22	0.16	0.08	2.673E+00	-0.20	0.02	-0.21
16	5.531E+03	1.940E+02	0.03	0.06	-0.02	2.779E+00	-0.43	0.03	-0.43
17	3.355E+03	3.136E+01	0.22	0.26	0.16	2.832E+00	-0.63	0.01	-0.63
18	2.500E+03	1.294E+01	0.24	0.25	0.18	3.018E+00	-1.70	-1.07	-1.71
19	1.234E+03	5.879E+00	-0.02	0.00	-0.02	2.925E+00	0.00	0.00	0.00
20	4.540E+02	3.418E+00	-0.06	0.00	-0.05	2.959E+00	0.00	0.00	0.00
21	6.144E+01	3.845E+00	-0.02	-0.01	-0.04	3.027E+00	-0.01	-0.02	-0.01

* Gray color denotes the resolved resonance region, and MC^2-2R represents the MC^2-2 calculation with RABANL option.

Table A.12 Comparison of Total Cross Sections for Cr-53 and Cr-54.

		Cr-53				Cr-54			
Group	Energy(eV)	VIM(barn)	VIM vs MC2-2(%diff)	VIM vs MC2-2R(%diff)	NJOY vs MC2-2(%diff)	VIM(barn)	VIM vs MC2-2(%diff)	VIM vs MC2-2R(%diff)	NJOY vs MC2-2(%diff)
1	1.414E+07	3.397E+00	-0.28	-0.28		3.397E+00	-0.28	-0.28	
2	6.065E+06	3.719E+00	-0.01	-0.01	0.23	3.746E+00	0.00	0.00	0.03
3	3.679E+06	3.722E+00	-0.06	-0.06		3.550E+00	-0.15	-0.15	
4	2.231E+06	3.423E+00	0.00	0.00	-0.04	3.527E+00	0.26	0.26	0.25
5	1.353E+06	3.537E+00	0.10	0.40	0.73	3.418E+00	-0.07	-0.31	1.79
6	8.209E+05	3.474E+00	-0.01	-1.72	0.04	3.885E+00	0.03	2.66	-0.17
7	4.979E+05	4.426E+00	-0.46	1.76	1.93	3.920E+00	-1.97	4.49	1.72
8	3.020E+05	4.422E+00	1.74	-0.78	2.44	3.778E+00	0.36	0.10	0.18
9	1.490E+05	6.321E+00	**4.68**	**-0.01**	**4.71**	8.058E+00	0.49	0.29	0.49
10	1.111E+05	8.542E+00	**2.80**	**-0.13**	**2.80**	3.379E+00	0.17	-0.07	0.16
11	6.738E+04	4.192E+00	**2.64**	**0.33**	**2.58**	4.723E+00	0.20	-0.06	0.23
12	4.087E+04	1.037E+01	**0.61**	**6.47**	**0.52**	6.523E+00	0.22	0.04	0.19
13	2.500E+04	8.657E+00	**0.62**	**7.09**	**0.61**	1.120E+01	0.20	0.20	0.24
14	1.503E+04	2.810E+01	**0.62**	**0.03**	**0.62**	5.746E+00	0.21	-0.02	0.22
15	1.000E+04	1.413E+02	**0.11**	**0.05**	**0.10**	4.915E+00	0.39	0.39	0.40
16	5.531E+03	1.825E+02	**-0.02**	**-0.17**	**0.00**	3.753E+00	0.00	0.01	0.00
17	3.355E+03	9.986E+01	0.23	0.27	0.17	3.200E+00	0.04	0.04	0.04
18	2.500E+03	3.932E+01	0.25	0.26	0.20	2.767E+00	0.04	0.04	0.03
19	1.234E+03	1.741E+01	-0.01	0.00	-0.02	2.487E+00	0.00	0.00	0.00
20	4.540E+02	1.027E+01	-0.06	0.00	-0.05	2.528E+00	0.00	0.00	0.00
21	6.144E+01	9.621E+00	-0.02	-0.01	-0.02	2.572E+00	-0.01	-0.02	-0.01

* Gray color denotes the resolved resonance region, and MC^2-2R represents the MC^2-2 calculation with RABANL option.

Table A.13 Comparison of Total Cross Sections for Fe-54 and Fe-56.

		Fe-54				Fe-56			
Group	Energy(eV)	VIM(barn)	VIM vs MC2-2(%diff)	VIM vs MC2-2R(%diff)	NJOY vs MC2-2(%diff)	VIM(barn)	VIM vs MC2-2(%diff)	VIM vs MC2-2R(%diff)	NJOY vs MC2-2(%diff)
1	1.414E+07	3.434E+00	-0.20	-0.20		3.540E+00	-0.20	-0.20	
2	6.065E+06	3.627E+00	-0.01	-0.01	-0.04	3.672E+00	-0.02	-0.02	0.23
3	3.679E+06	3.516E+00	-0.04	-0.04		3.226E+00	0.30	0.30	
4	2.231E+06	3.274E+00	-0.10	-0.10	-0.26	2.986E+00	0.29	0.29	0.28
5	1.353E+06	3.025E+00	0.28	0.67	-0.58	2.610E+00	-0.57	-0.42	0.41
6	8.209E+05	4.132E+00	-0.12	-1.01	0.48	2.955E+00	-0.23	0.80	-0.69
7	4.979E+05	4.328E+00	-1.38	-1.21	0.67	3.475E+00	0.92	-2.81	-4.10
8	3.020E+05	5.947E+00	0.66	-0.24	1.30	3.513E+00	0.35	-0.55	0.84
9	1.490E+05	3.036E+00	-1.29	-1.96	-1.40	4.029E+00	-0.07	0.12	-0.08
10	1.111E+05	4.522E+00	0.57	-0.55	0.78	5.282E+00	0.18	-0.03	0.15
11	6.738E+04	6.255E+00	0.62	0.22	0.52	4.166E+00	0.08	-0.16	0.12
12	4.087E+04	2.831E+00	1.04	-0.15	0.96	1.883E+01	0.09	-0.04	-0.01
13	2.500E+04	7.446E+00	0.50	-0.03	0.45	1.706E+00	0.37	-0.10	0.35
14	1.503E+04	2.368E+01	0.32	0.10	0.32	3.659E+00	0.18	-0.04	0.19
15	1.000E+04	1.170E+02	0.05	0.04	0.11	4.887E+00	0.22	0.02	0.21
16	5.531E+03	1.231E+00	0.09	0.14	-0.01	6.113E+00	0.24	0.03	0.24
17	3.355E+03	1.504E-01	-0.83	-0.96	-0.90	7.012E+00	0.18	-0.04	0.18
18	2.500E+03	7.869E-01	-0.22	-0.22	-0.23	8.134E+00	0.09	-0.14	0.09
19	1.234E+03	1.553E+00	0.01	0.00	0.00	9.987E+00	0.02	-0.03	0.03
20	4.540E+02	2.046E+00	0.02	0.00	0.02	1.137E+01	0.02	0.00	0.02
21	6.144E+01	2.376E+00	-0.02	-0.01	-0.02	1.224E+01	-0.01	-0.01	-0.01

* Gray color denotes the resolved resonance region, and MC^2-2R represents the MC^2-2 calculation with RABANL option.

Table A.14 Comparison of Total Cross Sections for Fe-57 and Fe-58.

		Fe-57				Fe-58			
Group	Energy(eV)	VIM(barn)	VIM vs MC2-2(%diff)	VIM vs MC2-2R(%diff)	NJOY vs MC2-2(%diff)	VIM(barn)	VIM vs MC2-2(%diff)	VIM vs MC2-2R(%diff)	NJOY vs MC2-2(%diff)
1	1.414E+07	3.540E+00	-0.20	-0.20		3.540E+00	-0.20	-0.20	
2	6.065E+06	3.672E+00	-0.02	-0.02	0.22	3.672E+00	-0.02	-0.02	0.22
3	3.679E+06	3.226E+00	0.30	0.30		3.226E+00	0.30	0.30	
4	2.231E+06	3.024E+00	0.22	0.22	0.13	3.024E+00	0.22	0.22	0.13
5	1.353E+06	2.672E+00	-0.06	-0.59	0.34	2.662E+00	-0.06	-0.43	0.35
6	8.209E+05	3.023E+00	-0.24	0.41	-0.59	3.013E+00	-0.24	0.60	-0.60
7	4.979E+05	3.579E+00	0.67	-1.32	-4.12	4.917E+00	-0.71	6.05	-1.30
8	3.020E+05	4.783E+00	0.17	-1.20	1.31	5.212E+00	0.04	0.70	-0.56
9	1.490E+05	1.095E+01	0.60	0.25	0.59	8.746E+00	0.21	0.13	0.28
10	1.111E+05	9.706E+00	0.46	-0.03	0.46	1.060E+01	0.05	0.29	0.02
11	6.738E+04	1.767E+01	0.19	0.17	0.18	2.247E+01	0.03	-0.23	0.00
12	4.087E+04	2.464E+01	0.11	-0.03	0.03	2.273E+00	0.60	0.41	0.53
13	2.500E+04	4.682E+00	**0.35**	**-0.03**	**0.36**	1.828E+00	0.48	-0.02	0.40
14	1.503E+04	4.048E+00	**1.26**	**-0.10**	**1.37**	2.562E+01	0.11	0.02	0.19
15	1.000E+04	5.501E+01	**0.28**	**0.13**	**0.25**	1.556E+00	0.04	-0.67	0.34
16	5.531E+03	3.239E+01	0.19	0.04	0.14	2.087E+00	0.78	0.09	0.79
17	3.355E+03	7.434E-01	**-2.07**	**-0.35**	**-2.06**	2.456E+00	0.76	0.04	0.76
18	2.500E+03	1.771E+00	**0.44**	**-0.35**	**0.51**	2.702E+00	0.78	-0.06	0.77
19	1.234E+03	2.246E+00	0.01	0.00	0.01	2.920E+00	0.93	-0.27	0.93
20	4.540E+02	2.532E+00	0.01	0.00	0.01	3.496E+00	0.62	-0.05	0.64
21	6.144E+01	2.809E+00	-0.02	-0.02	-0.02	3.199E+00	-0.01	-0.01	-0.02

* Gray color denotes the resolved resonance region, and MC^2-2R represents the MC^2-2 calculation with RABANL option.

Table A.15 Comparison of Total Cross Sections for Mn-55 and Mo-92.

		Mn-55				Mo-92			
Group	Energy(eV)	VIM(barn)	VIM vs MC2-2(%diff)	VIM vs MC2-2R(%diff)	NJOY vs MC2-2(%diff)	VIM(barn)	VIM vs MC2-2(%diff)	VIM vs MC2-2R(%diff)	NJOY vs MC2-2(%diff)
1	1.414E+07	3.469E+00	-0.20	-0.20		6.638E+00	0.01	0.01	
2	6.065E+06	3.708E+00	0.00	0.00	0.08	7.743E+00	-0.03	-0.03	-0.17
3	3.679E+06	3.642E+00	-0.06	-0.06		7.556E+00	-0.09	-0.09	
4	2.231E+06	3.464E+00	-0.03	-0.03	-0.28	6.962E+00	-0.06	-0.06	-0.30
5	1.353E+06	3.332E+00	0.08	-0.11	0.18	6.787E+00	-0.02	0.42	-0.35
6	8.209E+05	3.234E+00	0.07	-0.28	0.06	7.631E+00	0.03	-0.50	0.07
7	4.979E+05	3.868E+00	0.40	-1.41	-0.14	8.867E+00	-0.10	0.73	-0.01
8	3.020E+05	3.871E+00	0.00	-0.29	0.15	1.044E+01	0.00	-0.04	0.03
9	1.490E+05	7.107E+00	0.39	0.25	0.36	1.149E+01	0.00	0.00	0.00
10	1.111E+05	7.562E+00	-1.08	-0.08	-1.06	1.222E+01	**-1.54**	**-1.53**	**-0.11**
11	6.738E+04	8.511E+00	1.72	-0.01	1.75	1.308E+01	**-1.59**	**-1.06**	**-0.54**
12	4.087E+04	1.428E+01	0.68	0.02	0.76	1.384E+01	0.33	0.21	0.34
13	2.500E+04	1.308E+01	0.72	0.23	0.76	1.470E+01	0.38	0.18	0.49
14	1.503E+04	5.882E+00	1.20	0.14	1.21	1.553E+01	0.01	0.00	0.30
15	1.000E+04	4.184E+01	0.22	0.10	0.30	1.652E+01	0.09	-0.02	0.15
16	5.531E+03	1.190E+01	0.40	-0.09	0.42	1.769E+01	0.28	-0.13	0.42
17	3.355E+03	1.207E+02	-1.52	-1.74	-1.58	1.853E+01	1.68	1.69	1.50
18	2.500E+03	1.749E+02	0.43	0.46	0.40	2.125E+01	0.24	-0.04	0.25
19	1.234E+03	5.402E+01	0.27	0.33	0.21	2.750E+01	0.15	-0.02	0.17
20	4.540E+02	1.658E+02	-0.35	0.02	-0.25	4.159E+01	-0.10	-0.02	-0.08
21	6.144E+01	3.487E+00	0.00	0.01	-0.03	7.884E+01	-0.03	-0.04	-0.01

* Yellow color denotes the unresolved resonance region, gray color denotes the resolved resonance region, and MC^2-2R represents the MC^2-2 calculation with RABANL option.

Table A.16 Comparison of Total Cross Sections for Mo-94 and Mo-95.

		Mo-94				Mo-95			
Group	Energy(eV)	VIM(barn)	VIM vs MC2-2(%diff)	VIM vs MC2-2R(%diff)	NJOY vs MC2-2(%diff)	VIM(barn)	VIM vs MC2-2(%diff)	VIM vs MC2-2R(%diff)	NJOY vs MC2-2(%diff)
1	1.414E+07	4.113E+00	0.06	0.06		4.152E+00			
2	6.065E+06	3.826E+00	-0.01	-0.01	-0.15	3.841E+00			**-0.18**
3	3.679E+06	4.484E+00	-0.09	-0.09		4.281E+00			
4	2.231E+06	5.342E+00	-0.07	-0.07	-0.31	5.318E+00			**-0.30**
5	1.353E+06	6.531E+00	-0.02	0.79	-0.35	6.619E+00			**-0.36**
6	8.209E+05	7.786E+00	0.03	-0.51	0.06	7.981E+00			**0.07**
7	4.979E+05	8.661E+00	-0.10	0.73	-0.01	9.020E+00			**-0.04**
8	3.020E+05	9.228E+00	0.00	-0.04	0.03	9.592E+00			**-0.07**
9	1.490E+05	9.238E+00	0.00	0.00	0.00	9.538E+00			**-0.20**
10	1.111E+05	9.165E+00	**-1.43**	**-1.42**	**-0.11**	9.322E+00	Not Available		**-0.19**
11	6.738E+04	8.914E+00	**-1.99**	**-1.99**	**-0.12**	9.019E+00			**-0.17**
12	4.087E+04	8.657E+00	**-1.80**	**-1.80**	**-0.10**	8.772E+00			**-0.15**
13	2.500E+04	7.647E+00	-0.76	-0.61	-0.12	8.646E+00			**-0.12**
14	1.503E+04	1.009E+01	-0.16	0.23	-0.18	8.656E+00			**-0.10**
15	1.000E+04	7.234E+00	-0.10	-0.12	0.06	8.854E+00			**-0.07**
16	5.531E+03	1.307E+01	0.58	0.21	0.87	9.237E+00			**-0.06**
17	3.355E+03	5.514E+00	0.86	0.13	0.75	9.663E+00			**-0.06**
18	2.500E+03	8.686E+00	0.47	0.20	0.61	1.005E+01			**0.67**
19	1.234E+03	5.423E+00	0.41	-0.03	0.44	1.280E+01			**1.17**
20	4.540E+02	5.649E+00	0.26	-0.03	0.28	1.018E+01			0.95
21	6.144E+01	5.829E+00	-0.03	-0.03	-0.01	4.813E+01			0.61

* Yellow color denotes the unresolved resonance region, gray color denotes the resolved resonance region, and MC^2-2R represents the MC^2-2 calculation with RABANL option.

Table A.17 Comparison of Total Cross Sections for Mo-96 and Mo-97.

		Mo-96				Mo-97			
Group	Energy(eV)	VIM(barn)	VIM vs MC2-2(%diff)	VIM vs MC2-2R(%diff)	NJOY vs MC2-2(%diff)	VIM(barn)	VIM vs MC2-2(%diff)	VIM vs MC2-2R(%diff)	NJOY vs MC2-2(%diff)
1	1.414E+07	4.114E+00	0.06	0.06		4.113E+00	0.06	0.06	
2	6.065E+06	3.826E+00	-0.01	-0.01	-0.15	3.826E+00	-0.01	-0.01	-0.15
3	3.679E+06	4.484E+00	-0.09	-0.09		4.484E+00	-0.09	-0.09	
4	2.231E+06	5.342E+00	-0.07	-0.07	-0.31	5.342E+00	-0.07	-0.07	-0.31
5	1.353E+06	6.531E+00	-0.02	0.71	-0.35	6.531E+00	-0.02	0.66	-0.35
6	8.209E+05	7.786E+00	0.03	-0.53	0.07	7.786E+00	0.03	-1.03	0.07
7	4.979E+05	8.661E+00	-0.10	0.73	-0.01	8.661E+00	-0.10	0.74	-0.01
8	3.020E+05	9.228E+00	0.00	-0.04	0.03	9.228E+00	0.00	-0.04	0.03
9	1.490E+05	9.238E+00	0.00	0.00	0.00	9.238E+00	0.00	0.00	0.00
10	1.111E+05	9.181E+00	**-1.32**	**-1.31**	**-0.11**	1.004E+01	**-9.78**	**-9.77**	**-0.11**
11	6.738E+04	8.921E+00	**-1.75**	**-1.75**	**-0.12**	9.818E+00	**-10.73**	**-10.73**	**-0.12**
12	4.087E+04	8.694E+00	**-1.93**	**-1.93**	**-0.10**	9.366E+00	**-9.01**	**-9.00**	**-0.10**
13	2.500E+04	8.907E+00	**-0.97**	**-0.95**	**-0.06**	9.038E+00	**-7.18**	**-7.18**	**-0.05**
14	1.503E+04	9.936E+00	2.84	2.75	2.97	8.864E+00	**-5.65**	**-5.65**	**-0.09**
15	1.000E+04	1.010E+01	-1.11	-1.56	-1.13	8.844E+00	**-4.10**	**-4.10**	**-0.08**
16	5.531E+03	1.416E+01	0.64	0.27	0.87	9.070E+00	**-2.97**	**-2.97**	**-0.11**
17	3.355E+03	1.498E+01	0.89	0.79	1.09	9.392E+00	**-2.34**	**-2.34**	**-0.23**
18	2.500E+03	8.808E+00	1.06	0.80	0.67	1.080E+01	-0.44	-0.30	-0.15
19	1.234E+03	5.547E+00	0.47	-0.02	0.49	1.505E+01	1.47	0.78	1.22
20	4.540E+02	4.479E+01	0.37	0.93	0.32	1.126E+01	0.94	0.71	0.61
21	6.144E+01	4.692E+00	-0.04	-0.03	-0.01	6.664E+00	-0.04	-0.03	-0.01

* Yellow color denotes the unresolved resonance region, gray color denotes the resolved resonance region, and MC^2-2R represents the MC^2-2 calculation with RABANL option.

Table A.18 Comparison of Total Cross Sections for Mo-98 and Mo-100.

		Mo-98				Mo-100			
Group	Energy(eV)	VIM(barn)	VIM vs MC2-2(%diff)	VIM vs MC2-2R(%diff)	NJOY vs MC2-2(%diff)	VIM(barn)	VIM vs MC2-2(%diff)	VIM vs MC2-2R(%diff)	NJOY vs MC2-2(%diff)
1	1.414E+07	4.114E+00	0.06	0.06		4.259E+00	0.05	0.05	
2	6.065E+06	3.826E+00	-0.01	-0.01	-0.15	4.058E+00	-0.01	-0.01	-0.11
3	3.679E+06	4.485E+00	-0.10	-0.10		4.784E+00	-0.08	-0.08	
4	2.231E+06	5.342E+00	-0.06	-0.06	-0.31	5.652E+00	-0.06	-0.06	-0.30
5	1.353E+06	6.530E+00	0.00	0.65	-0.33	6.785E+00	-0.01	0.52	-0.31
6	8.209E+05	7.786E+00	0.03	-0.58	0.07	7.743E+00	0.02	-0.90	0.05
7	4.979E+05	8.661E+00	-0.10	0.73	-0.01	8.352E+00	-0.04	0.36	-0.07
8	3.020E+05	9.228E+00	0.00	-0.04	0.03	8.476E+00	0.00	0.00	0.00
9	1.490E+05	9.238E+00	0.00	0.00	0.00	8.421E+00	0.00	0.00	0.00
10	1.111E+05	9.127E+00	**-1.33**	**-1.32**	**-0.13**	8.549E+00	**-1.02**	**-1.02**	**0.18**
11	6.738E+04	8.831E+00	**-1.61**	**-1.61**	**-0.15**	8.369E+00	**-1.45**	**-1.45**	**0.04**
12	4.087E+04	7.955E+00	**-1.30**	**-0.88**	**-0.42**	8.400E+00	**-1.57**	**-1.56**	**-0.08**
13	2.500E+04	7.307E+00	-0.47	0.07	-0.51	1.068E+01	0.18	0.46	0.00
14	1.503E+04	9.711E+00	0.56	0.07	0.58	7.785E+00	0.95	-0.02	1.08
15	1.000E+04	1.155E+01	0.91	0.60	0.81	9.983E+00	0.99	0.32	1.00
16	5.531E+03	6.500E+00	0.52	-0.03	0.56	7.281E+00	0.86	0.12	1.09
17	3.355E+03	9.533E+00	1.34	0.71	1.42	9.609E+00	0.67	0.26	1.15
18	2.500E+03	9.072E+00	0.73	0.44	0.62	8.877E+00	-0.01	-0.45	0.57
19	1.234E+03	2.221E+01	1.48	1.22	1.05	6.400E+00	0.53	-0.03	0.57
20	4.540E+02	5.977E+00	0.48	0.06	0.56	1.510E+01	-0.09	0.53	0.07
21	6.144E+01	5.969E+00	0.17	0.01	0.18	5.289E+00	-0.03	-0.03	-0.01

* Yellow color denotes the unresolved resonance region, gray color denotes the resolved resonance region, and MC^2-2R represents the MC^2-2 calculation with RABANL option.

Table A.19 Comparison of Total Cross Sections for Ni-58 and Ni-60.

		Ni-58				Ni-60			
Group	Energy(eV)	VIM(barn)	VIM vs MC2-2(%diff)	VIM vs MC2-2R(%diff)	NJOY vs MC2-2(%diff)	VIM(barn)	VIM vs MC2-2(%diff)	VIM vs MC2-2R(%diff)	NJOY vs MC2-2(%diff)
1	1.414E+07	3.569E+00	-0.20	-0.20		3.636E+00	-0.17	-0.17	
2	6.065E+06	3.550E+00	-0.04	-0.04	-0.11	3.551E+00	0.01	0.01	-0.22
3	3.679E+06	3.244E+00	0.30	0.30		3.111E+00	0.00	0.00	
4	2.231E+06	3.157E+00	-0.01	-0.01	0.32	3.072E+00	-0.07	-0.07	0.42
5	1.353E+06	3.265E+00	-0.01	-1.04	1.38	3.303E+00	0.03	0.45	0.56
6	8.209E+05	3.313E+00	-0.44	0.57	-0.45	3.453E+00	-0.05	-1.57	-0.07
7	4.979E+05	4.415E+00	-0.33	-0.28	1.11	3.849E+00	-2.28	5.02	-3.99
8	3.020E+05	6.456E+00	0.93	0.25	0.91	4.653E+00	0.17	-0.40	0.55
9	1.490E+05	5.535E+00	-1.25	-1.70	-1.27	4.057E+00	0.67	0.02	0.70
10	1.111E+05	8.452E+00	0.12	-0.33	0.05	5.593E+00	0.38	0.14	0.37
11	6.738E+04	8.749E+00	-0.06	0.26	-0.14	6.937E+00	0.27	0.08	0.20
12	4.087E+04	1.092E+01	0.23	-0.07	0.19	1.497E+01	0.09	-0.01	0.05
13	2.500E+04	4.891E+01	0.10	-0.10	0.09	2.248E+01	0.05	-0.05	0.01
14	1.503E+04	1.078E+01	0.74	0.31	0.74	1.097E+02	-0.08	-0.07	-0.08
15	1.000E+04	9.769E+00	1.73	1.32	1.72	3.380E+00	-0.33	-0.38	-0.31
16	5.531E+03	1.502E+01	0.00	-0.01	0.00	7.200E-02	**15.71**	**0.28**	**15.86**
17	3.355E+03	1.768E+01	-0.03	-0.04	-0.04	2.708E-01	**2.24**	**-0.13**	**2.19**
18	2.500E+03	2.008E+01	-0.03	-0.03	-0.03	5.981E-01	0.27	-0.01	0.43
19	1.234E+03	2.259E+01	0.00	0.00	0.00	7.843E-01	0.00	0.00	0.00
20	4.540E+02	2.427E+01	0.01	0.00	0.01	9.523E-01	0.02	0.00	0.01
21	6.144E+01	2.519E+01	-0.01	-0.01	-0.01	1.221E+00	-0.02	-0.01	-0.03

* Gray color denotes the resolved resonance region, and MC^2-2R represents the MC^2-2 calculation with RABANL option.

Table A.20 Comparison of Total Cross Sections for Ni-61 and Ni-62.

		Ni-61				Ni-62			
Group	Energy(eV)	VIM(barn)	VIM vs MC2-2(%diff)	VIM vs MC2-2R(%diff)	NJOY vs MC2-2(%diff)	VIM(barn)	VIM vs MC2-2(%diff)	VIM vs MC2-2R(%diff)	NJOY vs MC2-2(%diff)
1	1.414E+07	3.652E+00	-0.16	-0.16		3.652E+00	-0.16	-0.16	
2	6.065E+06	3.621E+00	-0.03	-0.03	-0.09	3.621E+00	-0.03	-0.03	-0.09
3	3.679E+06	3.294E+00	0.11	0.11		3.294E+00	0.11	0.11	
4	2.231E+06	3.189E+00	-0.01	-0.01	0.39	3.189E+00	-0.01	-0.01	0.39
5	1.353E+06	3.286E+00	0.00	-0.22	1.12	3.286E+00	0.00	-0.22	1.12
6	8.209E+05	3.172E+00	-0.04	-0.40	-0.14	3.817E+00	-0.42	-2.46	-0.37
7	4.979E+05	4.262E+00	-0.64	1.82	-0.02	4.477E+00	-0.56	-0.44	-2.21
8	3.020E+05	5.954E+00	0.05	-0.17	0.22	3.979E+00	-1.11	0.49	-1.64
9	1.490E+05	5.214E+00	-0.22	-0.12	-0.27	7.224E+00	2.13	0.27	2.12
10	1.111E+05	8.314E+00	-0.18	-0.28	-0.15	5.437E+00	0.60	0.75	0.60
11	6.738E+04	7.641E+00	**-4.21**	**0.25**	**-4.26**	5.817E+00	0.44	0.08	0.39
12	4.087E+04	1.062E+01	**-1.72**	**0.14**	**-1.69**	5.413E+00	0.19	-0.03	0.15
13	2.500E+04	1.643E+01	**-2.28**	**0.08**	**-2.25**	1.026E+01	0.07	-0.02	0.02
14	1.503E+04	9.565E+00	**5.12**	**20.11**	**5.23**	2.166E+01	0.08	0.04	0.05
15	1.000E+04	2.112E+01	**-4.06**	**0.26**	**-4.01**	1.048E+02	0.16	0.12	0.02
16	5.531E+03	3.743E+00	-0.01	-0.02	0.01	4.263E+02	0.00	0.01	-0.01
17	3.355E+03	4.996E+00	-0.05	-0.06	-0.05	1.281E+02	0.26	0.31	0.21
18	2.500E+03	5.935E+00	-0.04	-0.04	-0.04	4.398E+01	0.28	0.29	0.23
19	1.234E+03	6.937E+00	0.00	0.00	0.00	1.893E+01	-0.02	0.00	-0.02
20	4.540E+02	7.657E+00	0.01	0.00	0.01	1.223E+01	-0.04	0.00	-0.04
21	6.144E+01	8.103E+00	-0.01	-0.01	-0.01	1.132E+01	-0.01	-0.01	-0.01

* Gray color denotes the resolved resonance region, and MC^2-2R represents the MC^2-2 calculation with RABANL option.

Table A.21 Comparison of Total Cross Sections for Ni-64 and Zr-90.

		Ni-64				Zr-90			
Group	Energy(eV)	VIM(barn)	VIM vs MC2-2(%diff)	VIM vs MC2-2R(%diff)	NJOY vs MC2-2(%diff)	VIM(barn)	VIM vs MC2-2(%diff)	VIM vs MC2-2R(%diff)	NJOY vs MC2-2(%diff)
1	1.414E+07	3.652E+00	-0.16	-0.16		4.106E+00	1.91	1.91	
2	6.065E+06	3.621E+00	-0.03	-0.03	-0.09	3.808E+00	**4.21**	**4.21**	**-0.10**
3	3.679E+06	3.294E+00	0.11	0.11		4.091E+00	**7.15**	**7.15**	
4	2.231E+06	3.189E+00	-0.01	-0.01	0.39	4.590E+00	**9.49**	**9.49**	**-0.25**
5	1.353E+06	3.286E+00	0.00	-0.57	1.12	5.638E+00	**10.56**	**11.13**	**-0.40**
6	8.209E+05	4.316E+00	-0.40	-3.41	-0.24	6.871E+00	**11.44**	**10.70**	**0.08**
7	4.979E+05	6.279E+00	0.30	-0.64	0.15	7.820E+00	**11.37**	**12.36**	**-0.07**
8	3.020E+05	7.378E+00	-0.32	-0.42	0.01	8.589E+00	**7.64**	**7.60**	**0.03**
9	1.490E+05	6.595E+00	1.64	-0.09	1.65	8.934E+00	**3.84**	**3.84**	**0.00**
10	1.111E+05	9.927E+00	0.41	-0.13	0.39	9.081E+00	**1.63**	**1.63**	**0.00**
11	6.738E+04	2.328E+01	0.12	-0.12	0.06	1.120E+01	0.17	-0.01	0.30
12	4.087E+04	3.835E+01	0.00	0.05	0.09	6.623E+00	0.39	-0.01	0.46
13	2.500E+04	3.181E+01	0.07	-0.12	0.03	1.203E+01	0.33	0.22	0.24
14	1.503E+04	7.520E+01	-0.09	-0.05	-0.10	7.882E+00	0.51	0.42	0.47
15	1.000E+04	4.532E+00	-0.19	-0.16	-0.18	6.493E+00	0.24	0.08	0.22
16	5.531E+03	8.332E-01	0.02	0.04	-0.04	1.113E+01	0.61	0.56	0.50
17	3.355E+03	3.494E-01	0.17	0.20	0.14	4.750E+00	-0.06	-0.07	-0.02
18	2.500E+03	1.623E-01	0.22	0.23	0.21	5.182E+00	-0.04	-0.04	0.00
19	1.234E+03	6.561E-02	-0.02	0.00	-0.01	5.346E+00	-0.03	-0.03	0.00
20	4.540E+02	4.359E-02	0.00	0.00	0.01	5.432E+00	-0.02	-0.03	0.00
21	6.144E+01	1.545E-01	-0.03	0.01	-0.08	5.486E+00	-0.03	-0.03	-0.01

* Yellow color denotes the unresolved resonance region, gray color denotes the resolved resonance region, and MC^2-2R represents the MC^2-2 calculation with RABANL option.

Table A.22 Comparison of Total Cross Sections for Zr-91 and Zr-92.

		Zr-91				Zr-92			
Group	Energy(eV)	VIM(barn)	VIM vs MC2-2(%diff)	VIM vs MC2-2R(%diff)	NJOY vs MC2-2(%diff)	VIM(barn)	VIM vs MC2-2(%diff)	VIM vs MC2-2R(%diff)	NJOY vs MC2-2(%diff)
1	1.414E+07	4.125E+00	0.00	0.00		4.125E+00	0.00	0.00	
2	6.065E+06	3.943E+00	0.00	0.00	-0.10	3.943E+00	-0.01	-0.01	-0.10
3	3.679E+06	4.326E+00	-0.04	-0.04		4.326E+00	-0.04	-0.04	
4	2.231E+06	4.850E+00	-0.06	-0.06	-0.23	4.850E+00	-0.06	-0.06	-0.23
5	1.353E+06	6.225E+00	-0.02	0.63	-0.51	6.225E+00	-0.02	1.02	-0.51
6	8.209E+05	7.882E+00	0.04	-0.66	0.09	7.882E+00	0.04	-0.67	0.09
7	4.979E+05	8.859E+00	-0.06	0.55	-0.06	8.859E+00	-0.06	0.55	-0.06
8	3.020E+05	9.294E+00	0.00	-0.04	0.03	9.294E+00	0.00	-0.04	0.03
9	1.490E+05	9.235E+00	0.00	0.00	0.00	9.231E+00	0.00	0.00	0.00
10	1.111E+05	1.007E+01	**-10.17**	**-10.17**	**-0.11**	9.013E+00	-1.40	-1.23	-0.26
11	6.738E+04	9.865E+00	**-11.27**	**-11.27**	**-0.13**	1.140E+01	-0.44	-0.03	-0.27
12	4.087E+04	9.444E+00	**-9.63**	**-9.63**	**-0.09**	9.711E+00	0.17	0.03	0.21
13	2.500E+04	9.017E+00	**-4.91**	**-3.80**	**-1.17**	8.603E+00	0.62	0.10	0.72
14	1.503E+04	9.694E+00	0.62	0.09	0.59	9.092E+00	0.21	-0.20	0.43
15	1.000E+04	1.136E+01	1.16	0.27	1.07	1.941E+01	0.28	0.15	0.43
16	5.531E+03	9.261E+00	1.09	0.09	1.13	1.531E+01	0.62	0.51	0.70
17	3.355E+03	1.877E+01	0.66	0.27	0.50	5.527E+01	1.34	1.43	1.36
18	2.500E+03	2.090E+01	0.65	0.40	0.57	3.852E+00	-0.03	-0.30	-0.02
19	1.234E+03	1.223E+01	1.04	0.69	0.68	5.800E+00	-0.02	-0.03	0.00
20	4.540E+02	1.828E+01	-0.39	0.07	-0.13	6.716E+00	-0.01	-0.02	0.01
21	6.144E+01	9.723E+00	-0.03	-0.03	-0.01	7.105E+00	-0.03	-0.03	-0.01

* Yellow color denotes the unresolved resonance region, gray color denotes the resolved resonance region, and MC^2-2R represents the MC^2-2 calculation with RABANL option.

Table 4.23 Comparison of Total Cross Sections for Zr-94 and Zr-96.

		Zr-94				Zr-96			
Group	Energy(eV)	VIM(barn)	VIM vs MC2-2(%diff)	VIM vs MC2-2R(%diff)	NJOY vs MC2-2(%diff)	VIM(barn)	VIM vs MC2-2(%diff)	VIM vs MC2-2R(%diff)	NJOY vs MC2-2(%diff)
1	1.414E+07	4.125E+00	-0.01	-0.01		4.125E+00	0.00	0.00	
2	6.065E+06	3.943E+00	0.00	0.00	-0.10	3.943E+00	0.00	0.00	-0.10
3	3.679E+06	4.326E+00	-0.04	-0.04		4.326E+00	-0.04	-0.04	
4	2.231E+06	4.850E+00	-0.06	-0.06	-0.23	4.850E+00	-0.06	-0.06	-0.23
5	1.353E+06	6.225E+00	-0.02	1.03	-0.51	6.225E+00	-0.02	0.61	-0.51
6	8.209E+05	7.882E+00	0.04	-0.67	0.09	7.882E+00	0.04	-0.67	0.09
7	4.979E+05	8.859E+00	-0.06	0.55	-0.06	8.859E+00	-0.06	0.55	-0.06
8	3.020E+05	9.294E+00	0.00	-0.04	0.03	9.294E+00	0.00	-0.04	0.03
9	1.490E+05	9.233E+00	0.00	0.00	0.00	9.233E+00	0.00	0.00	0.00
10	1.111E+05	1.233E+01	0.55	-0.36	0.91	1.015E+01	-0.20	0.03	0.12
11	6.738E+04	1.107E+01	1.07	-0.06	1.22	7.715E+00	0.03	-0.06	0.34
12	4.087E+04	1.030E+01	-0.28	-0.05	-0.07	1.236E+01	-0.21	-0.41	0.60
13	2.500E+04	1.465E+01	0.50	0.11	0.74	9.142E+00	0.20	0.09	0.31
14	1.503E+04	9.163E+00	0.68	-0.21	0.90	5.182E+00	-0.02	-0.05	0.03
15	1.000E+04	1.446E+01	0.85	0.46	0.75	1.013E+01	0.10	-0.04	0.40
16	5.531E+03	6.400E+00	0.71	0.02	0.68	1.988E+01	0.55	0.53	0.72
17	3.355E+03	7.319E+00	0.54	-0.07	0.56	5.097E+00	0.12	-0.04	0.15
18	2.500E+03	8.891E+00	0.10	0.06	0.17	5.321E+00	0.12	-0.04	0.14
19	1.234E+03	8.054E+00	-0.02	-0.02	0.00	5.528E+00	0.12	-0.03	0.14
20	4.540E+02	8.461E+00	-0.02	-0.02	0.01	1.063E+01	-1.39	-0.59	-0.44
21	6.144E+01	8.609E+00	-0.03	-0.03	-0.01	5.706E+00	-0.03	-0.04	-0.01

* Gray color denotes the resolved resonance region, and MC^2-2R represents the MC^2-2 calculation with RABANL option.

Nuclear Engineering Division
Argonne National Laboratory
9700 South Cass Avenue, Bldg. 208
Argonne, IL 60439-4842

www.anl.gov

A U.S. Department of Energy laboratory managed by UChicago Argonne, LLC